



HAL
open science

A PtdIns(4)P-driven electrostatic field controls cell membrane identity and signalling in plants

Mathilde Laetitia Audrey Simon, Matthieu Pierre Platre, Maria Mar Marquès-Bueno, Laia Armengot, Thomas Stanislas, Vincent Bayle, Marie-Cécile Caillaud, Yvon Jaillais

► To cite this version:

Mathilde Laetitia Audrey Simon, Matthieu Pierre Platre, Maria Mar Marquès-Bueno, Laia Armengot, Thomas Stanislas, et al.. A PtdIns(4)P-driven electrostatic field controls cell membrane identity and signalling in plants. *Nature Plants*, 2016, 2 (7), pp.16089. 10.1038/nplants.2016.89 . hal-03687823

HAL Id: hal-03687823

<https://hal.science/hal-03687823>

Submitted on 3 Jun 2022

HAL is a multi-disciplinary open access archive for the deposit and dissemination of scientific research documents, whether they are published or not. The documents may come from teaching and research institutions in France or abroad, or from public or private research centers.

L'archive ouverte pluridisciplinaire **HAL**, est destinée au dépôt et à la diffusion de documents scientifiques de niveau recherche, publiés ou non, émanant des établissements d'enseignement et de recherche français ou étrangers, des laboratoires publics ou privés.



Distributed under a Creative Commons Attribution 4.0 International License



Published in final edited form as:

Nat Plants. ; 2: 16089. doi:10.1038/nplants.2016.89.

A PI4P-driven electrostatic field controls cell membrane identity and signaling in plants

Mathilde Laetitia Audrey Simon^{1,*}, Matthieu Pierre Platre^{1,*}, Maria Mar Marquès-Bueno¹, Laia Armengot¹, Thomas Stanislas¹, Vincent Bayle¹, Marie-Cécile Caillaud^{1,#}, and Yvon Jaillais^{1,#}

¹Laboratoire de Reproduction et Développement des Plantes, UMR 5667 CNRS/INRA/ENS-Lyon/ Université de Lyon, 46 allée d'Italie, 69364 Lyon Cedex 07, France

Abstract

Many signaling proteins permanently or transiently localize to specific organelles for function. It is well established that certain lipids act as biochemical landmarks to specify compartment identity. However, they also influence membrane biophysical properties, which emerge as important features in specifying cellular territories. Such parameters include the membrane inner surface potential, which varies according to the lipid composition of each organelle. Here, we found that the plant plasma membrane (PM) and the cell plate of dividing cells have a unique electrostatic signature controlled by phosphatidylinositol-4-phosphate (PI4P). Our results further reveal that, contrarily to other eukaryotes, PI4P massively accumulates at the PM, establishing it as a critical hallmark of this membrane in plants. Membrane surface charges control the PM localization and function of the polar auxin transport regulator PINOID, as well as proteins from the BRI1 KINASE INHIBITOR1 (BK11)/MEMBRANE ASSOCIATED KINASE REGULATORS (MAKRs) family, which are involved in brassinosteroid and receptor-like kinase signaling. We anticipate that this PI4P-driven physical membrane property will control the localization and function of many proteins involved in development, reproduction, immunity and nutrition.

Each membrane compartment has a unique identity and thereby recruits a specific set of proteins¹⁻³. It has been established for decades that these identities are acquired by the combined presence of specific lipid and protein molecules that act as biochemical landmark on each membrane. For example, small GTPases from the Rab and ADP ribosylation factor (ARF) family as well as Soluble N-ethylmaleimide-sensitive-factor Attachment protein

Users may view, print, copy, and download text and data-mine the content in such documents, for the purposes of academic research, subject always to the full Conditions of use: http://www.nature.com/authors/editorial_policies/license.html#terms Reprints and permissions information is available at www.nature.com/reprints.

#Correspondence and requests for materials should be addressed to Y.J. (yvon.jaillais@ens-lyon.fr) and M.C.C (marie-cecile.caillaud@ens-lyon.fr).

*These authors contributed equally to this work

Author contributions: M.S., M.P. and M.C.C produced and imaged the lipid and MSC reporter lines, M.S., M.P., M.C.C and T.S. imaged the KA1^{MARK1} reporter in various tissues and plant systems, M.S. and M.P. carried out the PAO and WM experiments, V.B. performed the FRAP experiments and helped with image quantification and acquisition, M.C.C. performed cytokinesis and *N. Benthamiana* experiments, M.S., M.M.M.B and L.A. performed yeast and lipid overlay experiments, M.M.M.B and L.A. produced and imaged the MAKRs-cYFP lines, M.S. produced and phenotyped the *EXP7::PID* lines, M.S., M.P., M.C.C and Y.J. conceived the study and designed experiments, M.S., M.P., M.C.C. and Y.J. wrote the manuscript.

The authors declare no competing financial interests.

Receptor (SNARE) families are important components that contribute to membrane identity¹. On the lipid side, major determinants that distinguish one membrane from another belong to the phosphatidylinositol phosphate family (also known as phosphoinositides or PIPs)⁴. These phospholipids have an inositol head group that can be phosphorylated at various positions on their polar head^{4,5}. Many organelles contain a specific combination of phosphoinositides, which therefore attract proteins containing PIP-interacting stereospecific domains^{3,5,6}. Furthermore, it is well established that phosphoinositide production, dynamics and localization are regulated by Rab, ARF and SNARE proteins and conversely, that the activity and localization of these regulators is under the control of PIPs¹.

More recently, it was also recognized that each membrane can additionally be distinguished by its own biophysical properties, including lipid packing, curvature and electrostatics⁷. While the importance of these parameters were acknowledged long ago by biophysicists using theoretical modeling and artificial membrane systems, tools to probe these particular membrane properties in vivo have only recently been developed and have seldom been used so far in plants. Plant membranes share many characteristics with other eukaryotes; nonetheless they have singular features, including the presence of unique lipids (e.g. phytosterols, highly polar phytosphingolipids, galactolipids)⁸⁻¹⁰ and a drastically different endomembrane system (e.g. presence of chloroplasts, plasmodesmata, several vacuoles, a unique compartment that serves as trans-Golgi Network (TGN) and early endosome)¹¹⁻¹⁵.

Here, we began to address how membrane biophysical properties contribute to membrane identity in plants. In particular we analyzed the importance of membrane electrostatics in organelle identity and protein localization. Electrostatic interactions with negatively charged membrane contribute to the localization of many proteins containing polybasic clusters or cationic domains¹⁶⁻¹⁸. Membrane surface charges (MSC) are carried by anionic phospholipids^{7,18}. MSC are not evenly distributed throughout the cell but they are rather organized in specific cellular territories^{7,19}. How MSC are distributed and organized in plants is unknown. Using a set of surface charge biosensors, we found that the plant PM and the cell plate of dividing cells are highly electronegative as compared to endomembranes. Our results further revealed that the specific electrostatic field of the PM is lost upon chemical or genetic depletion of PI4P and that it contributes to the PM localization and function of several proteins involved in hormone and receptor-like kinase signaling.

Results

The plant PM has a specific electrostatic signature

In order to address the importance of membrane electrostatics in plants, we set out to map MSC in vivo, in Arabidopsis root epidermis. We raised a set of transgenic lines that constitutively express a mCITRINE (cYFP) fluorescent protein fused to a C-terminal farnesyl anchor in conjunction with an adjacent unstructured peptide of varying net positive charges (Extended Data Fig. 1)^{16,19}. The least cationic probe (8Q-Farn, 0+) was localized in numerous endomembrane compartments (Fig. 1a, p and Extended Data Fig. 1). Increasing electrostatic interactions by the gradual addition of lysines (cationic charges) targeted the probes to the PM at the expense of endomembrane localization (Fig. 1a-e, p, Extended Data Fig. 1). Probes of intermediate charges (4+ to 6+) clearly associated with the PM and labeled

few endomembrane compartments (Fig. 1c–d, p and Extended Data Fig. 1), which presumably are of intermediate electronegativity (Fig. 1q and Extended Data Fig. 1). The most cationic probe (8K-Farn, 8+) was strictly localized at the PM (Fig. 1e, p and Extended Data Fig. 1). To confirm the importance of the charges in the localization of our biosensors, we substituted the lysines within the cationic stretch with either arginine (8R-Farn, 8+, Fig. 1f) or glutamic acid (6K2E, 4+; 7K1E, 6+, Fig. 1g–h). Consistently, the probes with identical net charges showed a similar localization (Fig. 1c–h, p).

Next, we tested the effect of adding an adjacent polybasic sequence to different lipid anchors (Extended Data Fig. 1). Probes that were either geranylgeranylated (8Q-Gege, 0+) or myristoylated (Myr-8Q, 0+) were mainly localized in endomembrane compartments (Fig. 1i–j, p, Extended Data Fig. 1). By contrast, the 8+ probes (8K-Gege and Myr-8K, 8+) were specifically localized to the PM, supporting the notion that strong electrostatic interactions provide PM specificity regardless of the lipid anchor (Fig. 1k–l, p, Extended Data Fig. 1). Next, we expressed two cationic amphipathic helices that do not rely on lipid anchors for membrane association (the synthetic KRΦ sequence, 8+ and the C-terminal tail of the human GTPase Rit (Rit-tail), 9+, Extended Data Fig. 1)^{16,17}. Both probes were strictly localized to the PM (Fig. 1m–n, p). We also assayed the localization of the Kinase Associated-1 domains (KA1) of the human MARK1 (KA1^{MARK1}) and yeast Kcc4p proteins (KA1^{Kcc4p})²⁰. KA1 is a folded domain that lacks stereo-specificity and associates non-specifically with every anionic lipids^{20,21}. Consistent with our peptide-based probes, both KA1 domains localized specifically to the PM (Fig. 1o, p and Extended Data Fig. 1). Altogether, our results indicate that the PM of Arabidopsis root epidermal cells has a strong electrostatic-field, a unique and intrinsic property of this membrane that contributes to its identity (Fig. 1q). Interestingly, both 8K-Farn and KA1^{MARK1} MSC probes were insensitive to the cycling inhibitor Brefeldin A (BFA) (Extended Data Fig. 1), suggesting that high PM electrostatics does not require endocytic recycling. In addition, this property is not restricted to the root epidermis and was confirmed in other Arabidopsis cell types and in *Nicotiana benthamiana* (Extended Data Fig. 2).

PI4P is present early during cell plate formation, which correlates with the acquisition of a distinctive electrostatic state at the surface of this membrane

In animal cells, PM MSC are controlled by phosphatidylinositol-4,5-bisphosphate (PI(4,5)P₂), a phosphoinositide that localizes specifically at this membrane^{3,17,21}. However, PI(4,5)P₂ is necessary but not sufficient to maintain PM electrostatics^{17,21}. Indeed, depletion of PI(4,5)P₂ alone does not perturb PM MSC^{17,21}. However, concomitant depletion of PI(4,5)P₂ together with phosphatidylinositol-4-phosphate (PI4P)²¹ or phosphatidylinositol-3,4,5-bisphosphate (PI(3,4,5)P₃)¹⁷ triggers loss of PM MSC. PI(3,4,5)P₃ does not exist in plants^{3,22}, but PI(4,5)P₂ and PI4P both localize at the PM^{3,22–24} and are therefore potential anionic phospholipid candidates that might regulate PM electrostatics either alone or in combination. PI4P and PI(4,5)P₂ have both been reported to localize preferentially on the apical and basal poles of root epidermal cells rather than on their lateral sides^{25,26}. To analyze whether the localization of our MSC reporters correlates with the reported polar localization of phosphoinositide reporters^{25,26}, we determined their polarity indices (Extended Data Fig. 3). However, contrarily to previous reports^{25,26}, our

analysis suggested that phosphoinositides reporters are not differentially localized as compared to non-polar controls (Extended Data Fig. 3). We favor the hypothesis that confocal images of root cells might be biased for apical/basal signal over lateral signal because of the topology of these cells (see Extended Data Fig. 3). Next, to analyze whether MSC could be regulated preferentially by PI4P and/or PI(4,5)P₂, we analyzed MSC and the localization of these phosphoinositides during cytokinesis. In tobacco BY-2 cells, PI4P is present early during cell plate formation, while PI(4,5)P₂ is recruited later^{23,24}. We confirmed this observation using time-lapse imaging of Arabidopsis root meristem. To this end, we simultaneously localized our cYFP-tagged phosphoinositide sensors²² with the red dye FM4-64 as a cell plate marker¹³ or CENH3-RFP²⁷ as a chromosome marker (Extended Data Video 1 to 3). In addition, we concomitantly visualized a PI4P sensor in cyan (2xCyPet-1xPH^{FAPP1}) and a PI(4,5)P₂ sensor in yellow (cYFP-2xPH^{PLC})²² in the same roots and confirmed that PI4P is recruited to the cell plate much earlier than PI(4,5)P₂ (Fig. 1r and Extended Data Video 4 and 5). Next, we imaged our MSC sensor cYFP-KA1^{MARK1} together with FM4-64, CENH3-RFP or 2xCHERRY-1xPH^{FAPP1} and found that our MSC probe is recruited to the cell plate at the same time as PI4P (Fig. 1s and Extended Data Video 3 and 6 to 8). Together, these results suggest that PI(4,5)P₂ is dispensable for the establishment of a high electrostatic field, at least at the cell plate. By contrast, PI4P accumulation correlates with high membrane electrostatics at the PM and cell plate, suggesting that it could be important for MSC.

PI4-Kinase activity is required to maintain PM surface charges

To test this importance of PI4P in membrane electrostatics, we used short-term treatment of phenylarsine oxide (PAO), a PI4-kinases (PI4Ks) inhibitor (Fig. 2a)^{21,23,28}. We found that PAO triggers dissociation of PI4P-biosensors from the PM into the cytosol, while it had no or little effect on the PM localization of phosphatidylserine (PS) and PI(4,5)P₂ biosensors^{19,22} (Fig. 2b–i and Extended Data Fig. 4). This later result suggested that short-term inhibition of PI4Ks did not have a strong impact on PI(4,5)P₂ synthesis, although we found, as expected, that longer-term PAO treatment dissociated partially PI(4,5)P₂ from the PM (Extended Data Fig. 4). Likewise, short-term PAO treatment in mammalian cells inhibits PI4P production without severely affecting PI(4,5)P₂ level²¹. Similar to PI4P biosensors, PAO triggered the dissociation from the PM of our MSC sensor KA1^{MARK1} (Fig. 2f–g, j–o and t), in a time and dose-dependent manner. In addition, PAO also dissociated the MSC reporters Rit-Tail and KRΦ from the PM (Extended Data Fig. 4). These results suggest that PI4K activity plays a critical role in the PM electrostatic field. We confirmed these results using Wortmannin (WM), an inhibitor of PI3-kinases (PI3Ks) and PI4Ks at high concentration (>30 μM) but only of PI3Ks at low concentration (1 μM)(Fig. 2a)^{29,30}. As a control, we also used LY294002 that inhibits PI3Ks but not PI4Ks (Fig. 2a)³¹. We exploit our lipid biosensors²² to assess the effect of these drugs on PI3P, PI4P, PI(4,5)P₂ and PS (Extended data 4). Treatments at 30 μM WM dissociated both our PI4P biosensors and our MSC probe KA1^{MARK1} from the PM (Fig. 2s–t and Extended Data Fig. 4), albeit less effectively than PAO, while they had no effect on the PM localization of PI(4,5)P₂ and PS sensors (Extended Data Fig. 4). However, neither LY294002 nor 1 μM WM dissociated KA1^{MARK1} from the PM, confirming that PI4K but not PI3K activity is required for PM MSC (Fig. 2p–r, t and Extended Data Fig. 4). Live imaging in dividing cells together with

our pharmacological approaches suggest that PI4P, which is produced by PI4Ks, might be critical for PM electrostatics.

PI4P massively accumulates at the plant PM

PI(4,5)P₂ in mammals and PS in yeasts are major determinants of PM MSC^{16,17,19–21}. In both cases, these lipids specifically localize at the PM, thereby providing a specific electrostatic signature to this membrane. In plants, PI4P accumulates at the PM and endomembranes, as visualized by the PI4P biosensor 1xPH^{FAPP1} (Fig. 2g)^{22,23,32,33}. This raised the question of how PI4P might specifically control PM electrostatics while harboring such a binary localization. To probe whether PI4P preferentially accumulates at the PM, we compared the localization of three biosensors with increasing PI4P avidity. Increasing the number of PH^{FAPP1} domains increases the dwell time of the sensor in PI4P-riched membranes (Extended Data Fig. 5)^{3,22}, as confirmed by Fluorescent Recovery After Photobleaching (FRAP) experiments (Fig. 3a–c). Accordingly, 3xPH^{FAPP1}, and to a lesser extent 2xPH^{FAPP1}, preferentially localize to the PM rather than endosomes (Fig. 3d–f and i). Consistently, we previously found that PH^{OSBP}, another PI4P-binding protein, had a strict PM localization²² (Fig 2g, i). To confirm these findings, we used the recently described P4M domain from the *Legionella pneumophila* SidM protein, which was elegantly demonstrated as an exquisitely specific PI4P biosensor in vivo³⁴. In mammalian cells, P4M^{SidM} highlights several PI4P pools, including a main pool in the Golgi/TGN, and two relatively minor pools at the PM and endolysosomes³⁴. In contrast, P4M^{SidM} was strictly localized at the PM in *Arabidopsis* and in *Nicotiana benthamiana* leaf epidermis (Fig. 3h–j and Extended Data Fig. 6). The localization of the PH domain of FAPP1 relies on coincidence binding with both PI4P as well as the ARF1 small GTPase^{3,35}. In plants, ARF1 localizes to endosomes³⁶ and might account for the endomembrane localization of 1xPH^{FAPP1}. However, the fact that 1xPH^{FAPP1} also accumulates at the PM in plants, a compartment that lacks the ARF1 proteins, further suggest that PI4P accumulates to a significant extent in this membrane. Moreover, PH^{FAPP1} has two distinct binding sites for PI4P and ARF1, which can be mutated independently to specifically impair binding with one or the other molecule in vitro³⁵. We tested these mutants in vivo using transient expression in *N. benthamiana* leaf epidermis (Fig 3k–o). We found that mutants impaired in PI4P binding did not localized at the PM but in the cytosol as well as endomembranes, likely because of binding to ARF1 (Fig. 3l–m). On the contrary, PH^{FAPP1} version mutated in their ARF1-binding interface had a similar localization as P4M^{SidM}, being specifically localized at the PM and excluded from endomembranes (Fig. 3j and n–o). This result further exemplifies that PI4P is highly enriched at the PM in plants, which contrasts with other eukaryotic cells in which PI4P predominantly localizes to Golgi/TGN membranes and to a lesser extent at the PM³.

The pool of PI4P at the PM controls the surface charge signature of this membrane

Next, we built a genetic system to specifically deplete the PM PI4P pool and test its importance in PM MSC. In this system, we fused the active or inactive (DEAD) catalytic domain of the yeast Sac1p protein (a PI4P phosphatase) with the MAP (Myristoylation And Palmitoylation) sequence, which induces PM targeting in plants (Fig 4a)³⁷. To verify that our chimeric proteins were specifically targeted to the PM, we fused them to the cyan fluorescent protein mTURQUOISE2 and expressed them transiently in *N. Benthamiana*

(Fig. 4b–c). Next, we transiently co-expressed our chimeric enzymes together with our cYFP-tagged MSC probes or phosphoinositide markers. We found that MAP-SAC1, but not a catalytic mutant (MAP-SAC1^{DEAD}), displaced PI4P sensors to endosomes suggesting that our approach efficiently decreases PI4P concentration at the PM (Fig. 4d–e, i–j and n). However, we could not see any effects on the localization of our PI(4,5)P₂ biosensors (Fig. 4f, k and n). Importantly, we found that MAP-SAC1 perturbed the PM localization of the KA1^{MARK1} and 8K-Farn MSC markers, which were also found in endosomes in this condition (Fig. 4g–h and l–n). This experiment confirms two predictions: i) PI4P are much more concentrated at the plant PM than in endosomes and PI4P binding proteins localize to endosomes only when PI4P concentration at the PM is reduced and ii) PM PI4Ps are required to establish the high electrostatic property of the PM as compared to endomembranes. Our data therefore suggest that in plants, PI4P will confer endosomal localization to proteins that bind concomitantly to PI4P and to another endosome-localized partner (e.g. ARF1). However, it will target strict PI4P-binders specifically to the PM. Together, our results establish PI4P as a hallmark of the plant PM and a driving force behind the PM electrostatic field.

The PM electrostatic field drives the localization and function of a subset of hormone signaling proteins

Next, we asked whether endogenous Arabidopsis proteins might rely on the PM electrostatic field for their localization. The auxin transport regulator PINOID (PID) binds anionic lipids *in vitro*^{38,39} and is targeted to the PM via a polybasic unstructured loop within its kinase domain (PID membrane hook, PID^{MH}, 9+)³⁸. The negative regulator of the brassinosteroid receptor kinase, BRI1 KINASE INHIBITOR1 (BKI1), relies on a lysine-arginine-rich membrane hook for PM localization and function^{40,41}. We found that the cationic stretches in PID and BKI1 contribute to the interaction with anionic phospholipids *in vitro* and to their PM localization in yeast (Fig. 5a–b). Likewise, BKI1 family members (MEMBRANE ASSOCIATED KINASE REGULATORS, MAKR1 to MAKR4⁴⁰) also interacted with anionic lipids *in vitro* (Fig. 5a and Extended Data Fig. 7). Next, we took advantage of the yeast *cho1* mutant, which is impaired in PS biosynthesis¹⁹ and therefore lacks a strong PM electrostatic field²⁰. As a result of this loss of PM MSC in *cho1*, endomembranes become more electronegative than the PM and cationic proteins relocalize to endomembranes at the expense of their PM localization²⁰ (Extended Data Fig. 8). We confirmed that PID, BKI1 and MAKR1 to MAKR4 localized in endomembrane rather than the PM in *cho1*, while they associated with the PM in WT yeasts (Fig. 5b and Extended Data Fig. 8). In planta, MAKR1 to MAKR4 also associated with the PM via their polybasic N-termini (Extended Data Fig. 9). Next, we visualized MAKR2-cYFP and PID-YFP under the control of their endogenous promoter and found that they were targeted to the PM, although PID was also present in endomembrane compartments⁴² (Fig. 5c). These results are consistent with the notion that PID, MAKR2 and possibly other family members might localize to the PM by reading out its electrostatic field. Consistently, PID and MAKR2 localization were sensitive to PAO (Fig. 5c), indicating that their localization rely on PI4K activity.

Next, we tested the functional requirement of PID targeting at the PM by electrostatics. We took advantages of the PID^{9Q} membrane hook mutant (0+, Fig. 6a) that localizes to

endosomes but not at the PM (Fig. 6b). We adopted a gain-of-function strategy by specific overexpression of PID-cYFP (9+) in root-hair cells, which inhibits root hair elongation^{43,44} (Fig. 6c, h). By contrast, PID^{9Q}-cYFP (0+) overexpression in these cells had elongated root hairs (Fig. 6d, h). This phenotype resembled wild type (WT), PID^{D205N}-cYFP (kinase-dead) and 2xcYFP^{8K-Farn} control root hairs (8+, Fig. 6f), although they were slightly shorter (Fig. 6h). Because the membrane hook is in PID kinase domain (Fig. 6a), we could not exclude that the 9Q mutations might alter kinase activity, thereby preventing its function. We added a 5K3Q-Farn tail (5+, Extended Data Fig. 1) at the C-terminus of cYFP to target PID^{9Q} back at the PM and endosomes (Fig. 6e). This construct induced a short root hair phenotype that was statistically different from PID^{9Q} overexpression (Fig. 6e, h), suggesting that PID^{9Q} is a functional kinase and that, similar to BKI1^{40,41}, PID PM association by its cationic membrane hook is required for its function. This result further confirmed that PID is active at the PM rather than endomembranes³⁹.

Discussion

In this study we found that PI4P biosensors accumulate specifically at the PM in various cell types and in two plant species (i.e. *Arabidopsis thaliana* and *Nicotiana benthamiana*). Previous studies, using the PH domain of FAPP1, identified a pool of PI4P in endomembranes^{22,23}. We show that PH^{FAPP1} localization in endomembranes is due to coincidence binding of this domain with endosomal ARF1. This raised the question whether PI4P does accumulate in endosomes in plants. Multiple lines of evidence suggest that it does: i) PI4K β s localize in endosomes^{45,46} and ii) several Arabidopsis proteins that bind PI4P also localize in endomembranes^{47,48}. However, similar to PH^{FAPP1}, these proteins also bind both PI4P and endosomal small GTPases^{47,48}. In addition, we show that PI4P-binding domains that localizes specifically to the PM, also localizes to endomembranes upon depletion of the PI4P PM pool. This experiment suggests that there are two PI4P pools in plant cells that compete for the localization of PI4P-binding proteins: a major pool at the PM and a minor pool in endosomes (Fig. 4o). As a result, proteins that bind only to PI4P localize to the PM, while proteins that bind concomitantly to PI4P and an endomembrane protein are targeted to intracellular compartments. This organization of PI4P in two quantitatively different pools might therefore allow differential targeting of PI4P-binding proteins based on whether or not they bind additional molecules. It is important to bear in mind that PI4P biosensors can only associate with lipids that are not constantly occupied by endogenous PI4P-binding proteins (i.e. ‘unoccupied’ PI4P pool)³. It is therefore possible that a massive pool of PI4P is present in endomembranes but not available to target lipid sensors to this compartment (i.e. ‘occupied’ PI4P pool)⁴⁹. However, such occupied PI4P pool does not generate negative membrane charges, and is therefore not relevant for the generation of membrane electrostatic fields. In any case, in plant cells, the localization of ‘unoccupied’ PI4P that are labeled by biosensors, is drastically different from other eukaryotes, in which relatively equal pools of PI4P are detected at the PM and endomembrane inner surfaces³.

We found that accumulation of PI4P at the PM is essential to generate a high electrostatic field at this membrane. Our analyses in dividing cells suggest that PI(4,5)P₂ is dispensable for PM MSC. As such, PM MSC is differentially regulated in plants and animals^{17,19,21}. In the latter, PI(4,5)P₂ is required for the PM electrostatic field, but PI4P and/or PI(3,4,5)P₃ are

also important for the generation of high PM MSC^{17,21}. By contrast, in plants, loss of PM PI4P is sufficient to perturb membrane electrostatic properties. However, we cannot exclude that other anionic phospholipids such as PS or phosphatidic acid (PA) might also contribute to the PM electrostatic field. PA is not normally present at the PM in yeast and animal cells³, but it has been visualized in this membrane in plant tip-growing cells⁵⁰. Given that PA has two net negative charges, it could also be important for PM MSC. PS is the major anionic phospholipid at the yeast PM²⁰, but is also involved in PM electrostatics in animals¹⁹, in a non-redundant manner with phosphoinositides^{17,21}. Future studies will reveal whether PA and/or PS are involved, together with PI4P, in PM MSC.

We described several proteins involved in auxin, brassinosteroid and/or RLK signaling that rely on PM MSC for localization and function. There is a broad signaling potential behind this electrostatic localization mechanism¹⁸, since these interactions might be rapidly modulated by variations in: lipid composition (e.g. activation of phospholipases), the local cytosolic environment (e.g. ion influx) or modification of the protein itself. For example, phosphorylation of a conserved tyrosine within BKI1 membrane hook triggers PM dissociation⁴⁰, likely by acting as an electrostatic switch¹⁸. Here, we provide several examples of MSC effectors in Arabidopsis, but we expect that many more proteins will rely on this particular PM physical property for localization and function.

Methods

Growth condition and plant materials

The following transgenic lines: *pUBQ10::cYFP-1xPH^{FAPP1}*, *pUBQ10::cYFP-2xPH^{FAPP1}*, *pUBQ10::cYFP-PH^{OSBP}*, *pUBQ10::cYFP-2xPH^{PLC}*, *pUBQ10::2xCHERRY-1xPH^{FAPP1}*, *pUBQ10::2xCyPet-1xPH^{FAPP1}*, *35S::CENH3-RFP*, *35S::EGFP-Lti6b*; *35S::EGFP-aqPIP2a*; *PIN2::PIN2-EGFP* (Gift from Ben Scheres, Wageningen University, Netherland) and *pPID::PID-YFP* (Gift from Ji í Friml, Institute of Science and Technology, Austria) were described before^{22,27,36,42,51}. Arabidopsis Col0 accession were grown in soil under long-day conditions at 21°C and 70% humidity.

Root imaging and image quantification

Plant growth—For root imaging, seedlings were grown vertically on MS medium (pH 5.7) containing 0.8% plant agar (Duchefa, <http://www.duchefa-biochemie.nl/>) in the absence of sucrose, with continuous daylight for 6–9 days.

Microscopy setup—Plant imaging was performed on an inverted Zeiss microscope (AxioObserver Z1, Carl Zeiss Group, <http://www.zeiss.com/>) equipped with a spinning disk module (CSU-W1-T3, Yokogawa, www.yokogawa.com) and a ProEM+ 1024B camera (Princeton Instrument, <http://www.princetoninstruments.com/>) using a 63x Plan-Apochromat objective (numerical aperture 1.4, oil immersion). GFP was excited with a 488 nm laser (150mW) and fluorescence emission was filtered by a 525/50 nm BrightLine® single-band bandpass filter (Semrock, <http://www.semrock.com/>). YFP/cYFP were excited with a 515nm laser (60mW) and fluorescence emission was filtered by a 578/105 nm BrightLine® single-band bandpass filter (Semrock, <http://www.semrock.com/>), CyPet/

mTURQUOISE2 were excited with a 445nm laser (80mW) and fluorescence emission was filtered by a 482/35 nm BrightLine® single-band bandpass filter (Semrock, <http://www.semrock.com/>), CHERRY/RFP were excited with a 561nm laser (80mW) and fluorescence emission was filtered by a 609/54 nm BrightLine® single-band bandpass filter (Semrock, <http://www.semrock.com/>). All imaging experiments were performed with spinning disk confocal except FM-64 colocalizations, which were performed on an inverted Zeiss CLSM710 confocal microscope (time lapse of cell division, Extended Data Video 1, 2 and 6) or inverted Zeiss CLSM780 confocal microscope (BFA experiments of Extended Data Figure 1, Sigma, www.sigmaaldrich.com) and images from Extended Figure 1 which were acquired on an inverted Zeiss CLSM710 confocal microscope as previously described²².

For quantitative imaging, pictures of epidermal root meristem cells were taken with detector settings optimized for low background and no pixel saturation. Care was taken to use similar confocal settings when comparing fluorescence intensity. Pseudo-colored images were obtained using the “Green Fire Blue” look-up-table (LUT) of Fiji software (<http://www.fiji.sc/>).

Time lapse imaging of cell division in root meristem—Five days old Arabidopsis seedlings were transferred in a chambered cover glass (Lab-Tek II, <http://www.thermoscientific.com>), which contained 1.5 ml of MS medium (pH 5.7) containing 0.8% plant agar (Duchefa, <http://www.duchefa-biochemie.nl/>) in the absence of sucrose. Epidermal cells in the meristematic region of the root were subjected to time-lapse imaging with spinning disk confocal microscope, except for FM4-64 (Life Technologies, <http://www.thermofisher.com/>) colocalization. Colocalization analysis of cYFP-biosensor with FM4-64 was performed on an inverted Zeiss CLSM710 confocal microscope using a 63x Plan-Apochromat objective (numerical aperture 1.4, oil immersion). Counter-staining of the plasma membrane was obtained by incubating roots with 1 μ M FM4-64 solution during the entire time course. cYFP and FM4-64 were excited with a 515 nm laser and detected with microscope settings described in⁴⁴. Two or three roots were observed simultaneously and images were collected at different Z-positions every 3 min (spinning disk) or 4 min (CLSM). All the Time-lapse were adjusted for growth using the Template Matching and Slice Alignment (ImageJ Plugins, <https://sites.google.com/site/qingzongtseng/template-matching-ij-plugin>). In figure 1, t=0 min was determined as the frame preceding the first image with cell plate labeling in the PI4P reporter channel (t=3 min).

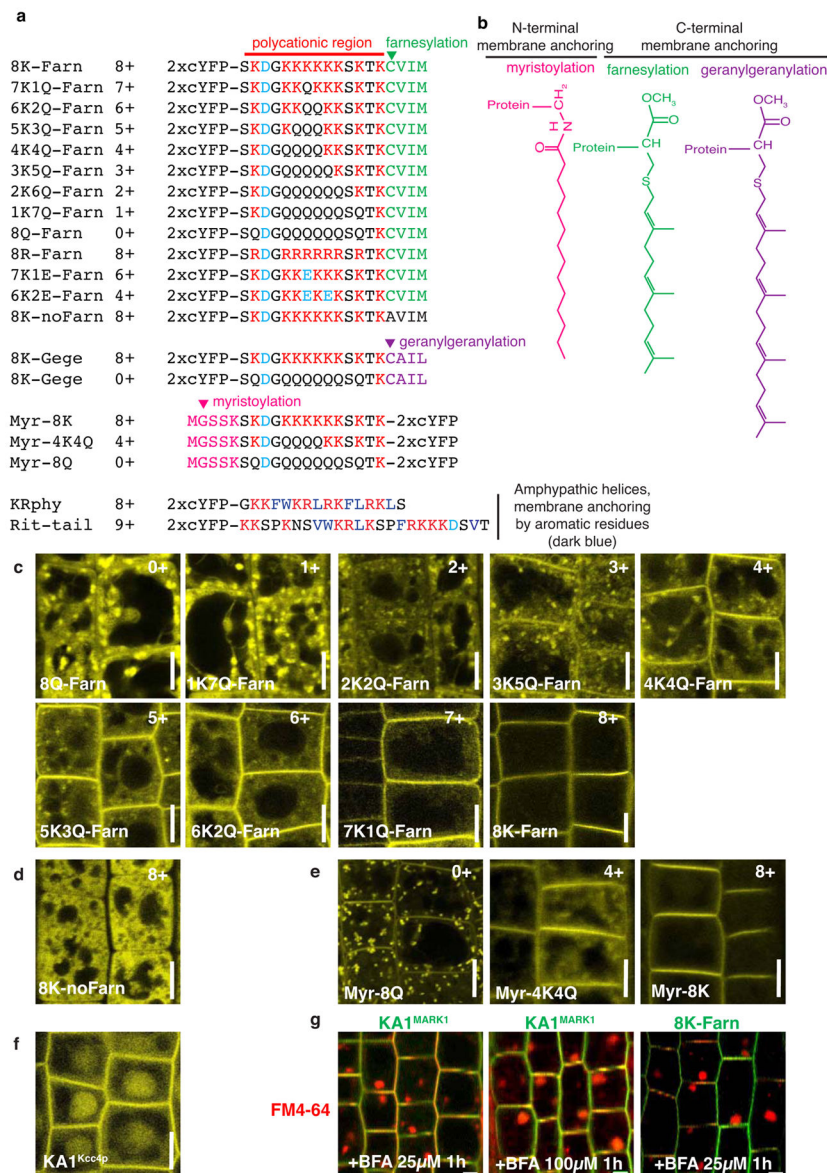
Quantification of the number of intracellular compartments (“spots”) per cell—The intracellular compartments (“spots”) per cell were counted in a double blind setup. 100 cells were counted per condition, in at least 20 independent roots imaged over the course of at least 3 independent experiments. For the MAP-SAC1 experiments in agro-infiltrated *Nicotiana Benthamiana* leaves quantifications were performed by counting the number of cells with endomembrane labeling (presence of cytosolic “spots”) and the number of cells showing only PM labeling. Minimums of 100 cells were counted in each condition over the course of at least three independent experiments.

PAO, WM and LY294002 treatments and dissociation index—7-day old transgenic lines (cYFP-1xPH^{FAPP1}, cYFP-C2^{Lact}, cYFP-2xPH^{PLC}, cYFP-KA1^{MARK1}, cYFP-2xFYVE^{HRS}, pMAKR2::MAKR2-cYFP and pPID::PID-YFP or the following F2 crosses 2xCHERRY-C2^{Lact}xcYFP-1xPH^{FAPP1}; cYFP-2xPH^{PLC}x2xCyPet-1xPH^{FAPP1}; cYFP-KA1^{MARK1}x2xCHERRY-1xPH^{FAPP1}) were incubated in wells containing 30 μ M or 60 μ M PAO (Sigma, www.sigmaaldrich.com, PAO stock solution at 60 mM in DMSO), 1 μ M or 30 μ M PAO (Sigma, www.sigmaaldrich.com, WM stock solution at 30 mM in DMSO), 50 μ M LY294002 (Cayman chemical, <https://www.caymanchem.com>, LY29002 stock solution at 50 mM in DMSO), or a volume of DMSO equivalent to the highest drug concentration used in each case (mock treatment) during the indicated time. Roots were imaged within a 10 min time frame window around the indicated time. The PAO, WM and LY29002 effects on the localization of our biosensors were analyzed by calculating the “dissociation index” for each reporter protein²¹. First, we calculated “indexMock”: the ratio between the fluorescence intensity (Mean Grey Value function of Fiji software) measured in two elliptical region of interest (ROIs) from the plasma membrane region (one at the apical/basal PM region and one in the lateral PM region) and two elliptical ROIs in the cytosol in the mock condition. “IndexMock” was quantified in 150 cells over three independent replicates (50 cells per replicate). Next, we measured a similar ratio in drug treated seedlings (“indexDrug”). “indexDrug” was also quantified in 150 cells over three independent replicates (50 cells per replicate). The dissociation index is the ratio of (indexMock)/(indexPAO). This dissociation index reveals the degree of relocalization of the fluorescent reporters from the plasma membrane to the cytosol, between the mock and drug treated conditions.

For the quantification of the PAO effect on PID-YFP and MAKR2-cYFP localization, we did not use a dissociation index, because the localization of these two proteins was already high in the cytosol even in the absence of PAO. Therefore, to reflect the variability associated with protein localization, we scored, in a double blind setup, the number of cells in which PID-YFP or MAKR2-cYFP were associated or not with the PM in the mock and PAO treated conditions. In Figure 5, these scores are given as the number of cells with protein at the PM over the total number of cells (mock condition) and the number of cells with no protein at the PM over the total number of cells (PAO-treated condition).

FRAP experiment—Fluorescence in a rectangle region of interest (ROIs) (50 μ m², 15 μ m long), in the plasma membrane region, was bleached in root optical section by four successive scans at full laser power (150W) using the ilas² FRAP module (Roper scientific, <http://www.biovis.com/ilas.htm>) of our spinning disk microscope. Fluorescence recovery was subsequently analyzed in the bleached ROIs and in controlled ROIs (rectangle with the same dimension, in unbleached area). FRAP was recorded continuously during 90s with a delay of 0.3s between frames. Fluorescence intensity data were normalized as previously described³⁷. For visualization, kymographs were obtained using the kymograph function of the Metamorph software.

Extended Data



Extended Data Figure 1. Construction of membrane surface charge (MSC) probes and additional MSC reporters confirming the high electronegativity of the plasma membrane in plants

a) Sequence alignment between the different MSC probes showing the polybasic stretch in each construct (or the associated mutations) and their respective net positive charges. Cationic residues (K, R) are in red, acidic residues (E, D) in light blue, hydrophobic and aromatic residues in the amphipathic helices Rit-tail and KRphy are in dark blue (F, W, L, V), the C-terminal farnesylation sequence CVIM (CxxM box) is in green, the C-terminal geranylgeranylation sequence CAIL (CxxL box) is in purple and, the N-terminal myristoylation sequence MGSSK is in pink.

b) Schematic representation of the lipid modifications used in our MSC probes: myristoyl (pink, N-terminal modification, covalently linked to the second glycine), farnesyl (green, C-terminal modification, covalently linked to the cysteine in the CxxM motif) and geranylgeranyl (purple, C-terminal modification, covalently linked to the cysteine in the CxxL motif).

c–f) Representative confocal images of root epidermal cells expressing the indicated MSC probe. All the constructs are expressed by the *pUBQ10* promoter and are fused with cYFP at their N-terminus, except the myristoylated constructs, which are fused with cYFP at their C-terminus. bars, 5µm.

c) Localization of the full collection of farnesylated probes from 8Q-Farn (0+) to 8K-Farn (8+). The farnesylated MSC probes are based on the C-terminal tail of the human small GTPase K-Ras4B¹⁹. K-Ras is targeted to the PM via a C-terminal farnesyl anchor in conjunction with an adjacent unstructured polybasic peptides made of 8 lysines. Our bioprobes consist of a fusion between a tandem repeat mCITRINE fluorescent protein (cYFP) and the K-Ras C-terminal tail, in which we modified the net positive charges via site directed mutagenesis of the lysine stretch. The least cationic probe (0+), in which 8 lysines have been substituted by glutamine (8Q-Farn), is localized in numerous endomembrane compartments. This suggests that farnesylation of the 8Q-probe is sufficient to provide membrane anchoring in the absence of its adjacent lysines and that this probe, which is targeted mainly by hydrophobic interactions, confers targeting to intracellular membranes. The gradual addition of cationic charges should increase electrostatic interactions with anionic lipids and thereby shift the probes localization toward more negatively charged membranes. Indeed, we observed that the more cationic the probe is, the more it is targeted to the PM at the expense of endomembrane localization.

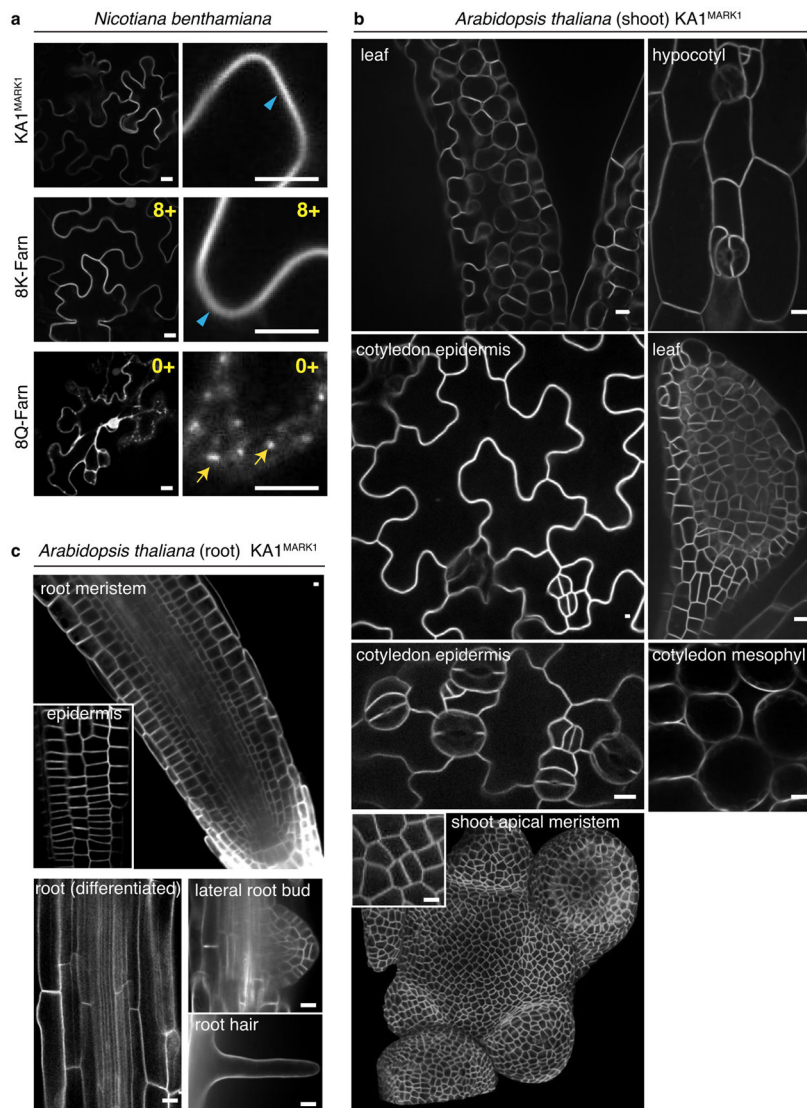
d) The cysteine in the CxxM motif of 8K-Farn was substituted by an alanine thereby prohibiting C-terminal addition of a farnesyl lipid anchor (8K-noFarn). This non-farnesylated probe failed to associate with any membrane and was fully soluble, despite being strongly cationic (8+). This suggests that electrostatic interactions by themselves are not sufficient for membrane targeting and that stable membrane association requires some type of hydrophobic interactions.

e) Localization of the Myr-8Q (0+), Myr-4K4Q (4+) and Myr-8K (8+) probes. Note that, by contrast with the 8Q-Farn (Extended Data Fig. 1c, top left panel) and 8Q-Gege probes (see main Fig. 1i), the Myr-8Q probe is already partly associated with the PM in the absence of electrostatic interactions. This showed that these different lipid anchors have different intrinsic targeting properties but that they each failed to provide PM specificity on their own. Nonetheless, like for the farnesylated reporters, the gradual addition of net positive charges next to the myristoyl modification gradually increases PM association: Myr-4K4Q (4+) has an intermediate PM/endomembrane localization and Myr-8K is specifically localized at the PM. Together, our results support the notion that strong electrostatic interactions provide PM specificity regardless of the lipid anchor type.

f) Localization of the KA1^{Kcc4p} reporter at the PM and in the nucleus. Similar to KA1^{MARK1}, KA1^{Kcc4p} is specifically localized at the PM and not in endomembrane compartments, confirming that this specific localization at the cell surface is a property of the KA1 domain in general rather than a specific feature of the MARK1 protein. However, unlike KA^{MARK1}, KA1^{Kcc4p} was also partly localized in the cytosol and the nucleus, which

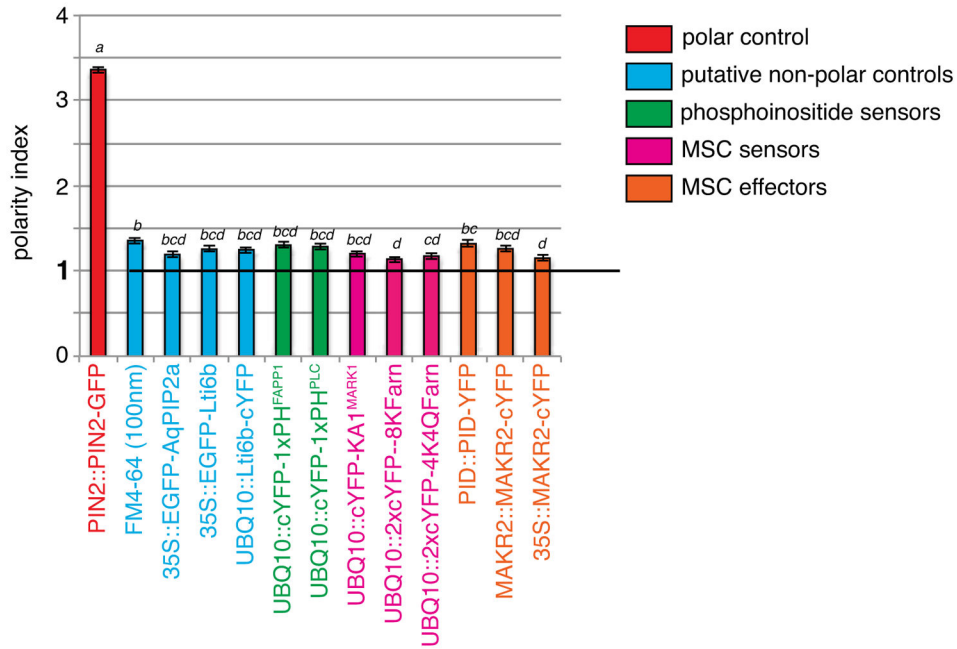
makes this domain less convenient as a MSC readout. For this reason, from now on, we decided to use the KA1^{MARK1} domain in subsequent experiments.

g) Sensitivity of KA1^{MARK1} (left and middle panel) and 8K-Farn (8+ probe, right panel) to 90 min of BFA treatment at the indicated concentration. To show that BFA was active during our treatment we used the endocytic tracer FM4-64 and found that it was accumulated in BFA bodies at both 25 μ M and 100 μ M of BFA. FM4-64 was used at 1 μ M and added 10 min prior confocal observations in the continuous presence of BFA.



Extended Data Figure 2. The high electronegativity of the PM is a common feature of many cell types and at least two plant species

a) Localization of KA1^{MARK1}, 8K-Farn (8+), 8Q-Farn (0+) in transiently transformed *N. benthamiana* leaves. Blue arrowheads show PM localization and yellow arrows show endomembrane localization. **b–c)** Confocal picture of **b)** the shoot and **c)** the root of transgenic *Arabidopsis* lines stably expressing cYFP-KA1^{MARK1}. Scale bars, 10 μ m.

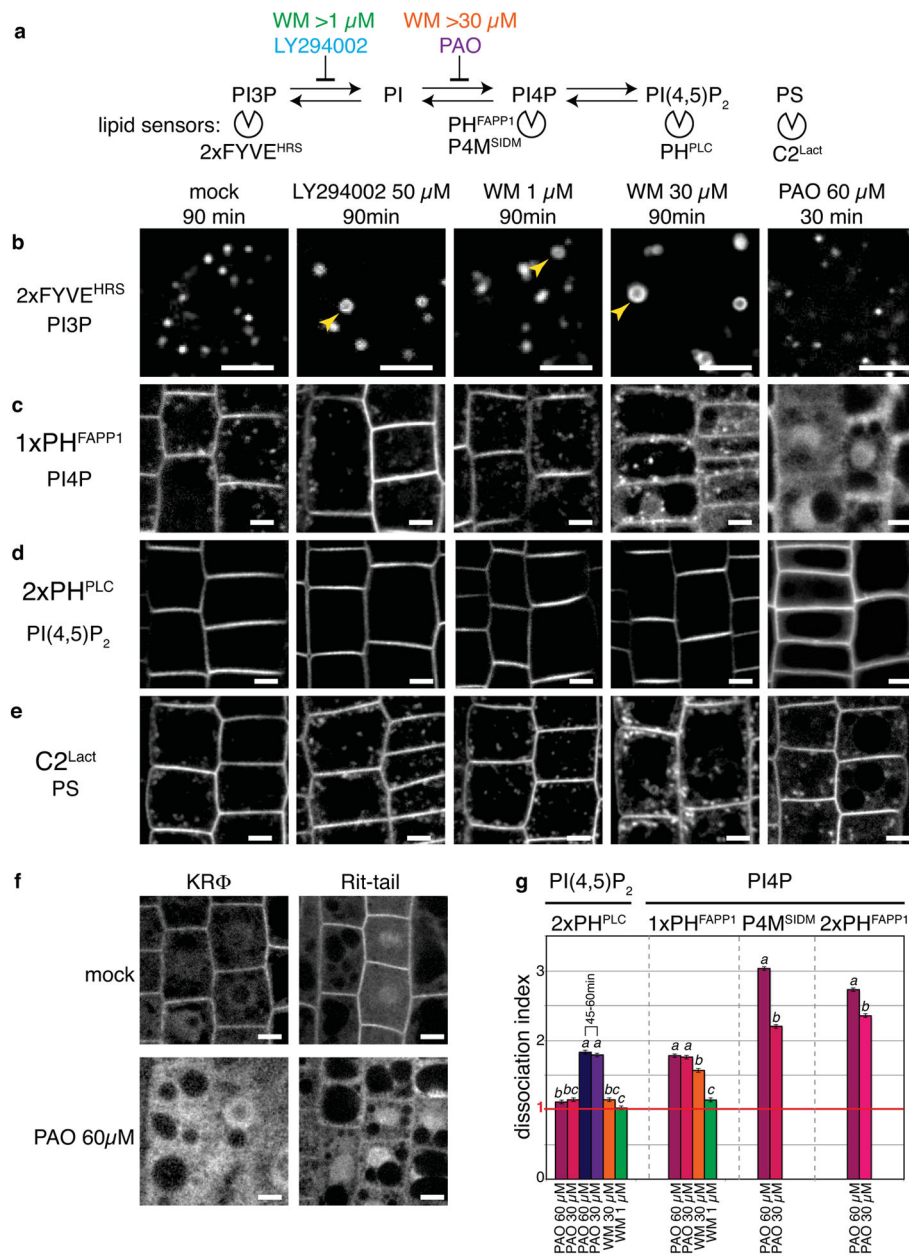


Extended Data Figure 3. Polarity indices in Arabidopsis root epidermis of various fluorescent PM proteins

Charts showing the polarity index for each fusion protein indicated at the bottom. Different italicized-letters indicate significant differences among means ($P < 0.0001$, Tukey's test). Note that only PIN2-GFP (red) is significantly different from all the other genotypes. The polarity indices of phosphoinositide (green) and MSC (pink) sensors fluctuate between 1.2 and 1.4, which is close to the numbers reported for PI4P and PI(4,5)P₂ reporters²⁰. However, we found that expected non-polar controls (blue), including the lipid dye FM4-64 and plasma membrane proteins Lti6b and PIP2a aquaporin (aqPIP2a) have similar polarity indices. Therefore, we could not detect significant statistical differences between our phosphoinositides or MSC sensors and expected non-polar controls. Although we cannot exclude that these non-polar control are in fact polar, we favor the hypothesis that confocal images of root cells might be biased for apical/basal signal over lateral signal because of the topology of these cells. First, the apical pole of one cell is tightly juxtaposed to the basal pole of its neighbouring cell, which tend to enhance the apparent apical/basal signal over the lateral one. In addition, pinhole-based microscopes have high thickness of the z-sections. As a result, the z resolution is much lower than x and y resolution, so the volume collected by the microscope is not an isodiametric cube but cuboid; therefore a straight membrane in z will appear stronger than a curved one - which is the case of the apical and basal root membranes compared to the lateral membranes. Therefore we concluded that phosphoinositides and PM MSC are likely not polar in Arabidopsis root epidermis.

Method for quantification of polarity index. 7 days old transgenic lines were analyzed to determine the "Polarity index" in root tip epidermis. "Polarity index" is the ratio between the fluorescence intensity (Mean Grey Value function of Fiji software) measured at the PM apical/basal side and PM lateral sides (Line width=3). We selected only cells for which the PM at each pole (apical, basal and laterals) were easily viewable and we selected cells that were entering elongation (at least as long as wide, but no more than twice as long as wide).

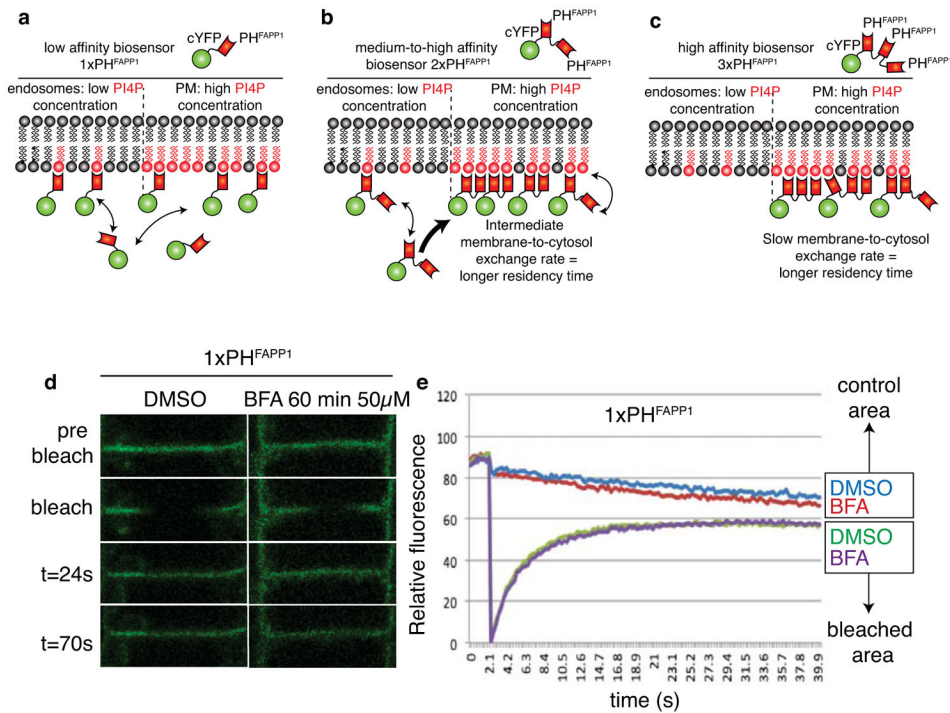
Quantification was conducted in 100 cells over more than 15 independent plants. This Polarity index reveals the degree of polarity of the fluorescent reporters between the apical/basal side and lateral sides of the PM.



Extended Data Figure 4. Sensitivity of phosphoinositides and MSC sensors to PI3K and PI4K inhibitors

a) Schematic representation of the action of the drugs used to perturb phosphoinositides production and lipid sensors used as read-out. **b–e)** Confocal pictures of Arabidopsis root epidermis from the genotype indicated on the left, treated with the drug concentration indicated at the top for 90 min (mock, LY294002 and WM) or 30 min (PAO).

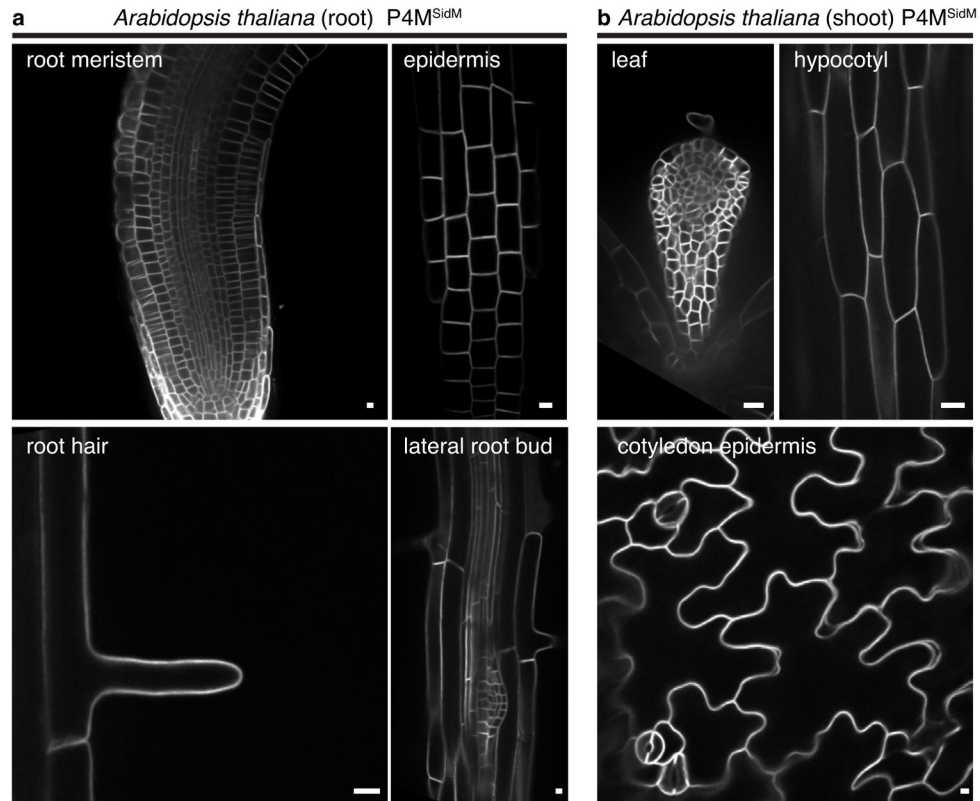
- b)** cYFP-2xFYVE^{HRS}. As reported previously, 90 min of PI3K inhibition leads to swelling of late endosomes labelled by the PI3P sensors 2xFYVE^{HRS}, rather than a release of the probe into the cytoplasm²¹. Yellow arrowheads show enlarged endosomes. Endosome swelling suggested that WM and LY294002 are active, although we noticed that WM had a more drastic effect at 30 μ M than 1 μ M. On the other hand, PAO treatment had no effect on 2xFYVE^{HRS}-labelled endosomes.
- c)** cYFP-1xPH^{FAPP1}. PI3K inhibition by LY294002 and 1 μ M WM had no effect on 1xPH^{FAPP1} localization. However PI3K and PI4K inhibition by 30 μ M WM partially released 1xPH^{FAPP1} into the cytosol and PI4K inhibition by PAO fully solubilized this PI4P sensor. In the 60 μ M 30 min PAO treatment (right) both the PM and endosomal pools of 1xPH^{FAPP1} were solubilized. This result is surprising given that the endosomal pool of 1xPH^{FAPP1} can rely only on ARF1-binding for endomembrane localization (See Fig. 3 of main text). The PH domain of FAPP1 interacts specifically with GTP-loaded ARF1²² and it is possible that PI4K inhibition inhibits ARF1 activation. For example, the ARF GTPase Activating Protein (ARF-GAP) VAN3, which binds ARF1 in Arabidopsis, has a PI4P-binding PH domain and its GAP activity is enhanced by PI4P²³.
- d)** cYFP-2xPH^{PLC}. Only PAO 60 μ M 30 min (right) had a slight effect on the PM localization of the PI(4,5)P₂ biosensor 2xPH^{PLC}, which becomes significant after prolonged treatment (45 to 60 min of 60 μ M PAO, see **g**).
- e)** cYFP-C2^{Lact}. Inhibition of PI3K and/or PI4K had no effect on the PM localization of the PS biosensor C2^{Lact}. However, we noticed that 60 μ M PAO for 30 min (right) decreased the number of endomembrane compartments labeled by this probe, suggesting some impact of PI4K activity on the intracellular localization of PS.
- f)** Confocal picture of Arabidopsis root epidermis from the genotype indicated at the top, treated with the drug concentration indicated on the left for 30 min.
- g)** Dissociation index (mean \pm SEM) for the genotype and drug concentration indicated at the bottom. All treatments were performed during 30 min, except when indicated otherwise. Different italicized-letters indicate significant differences among means ($P < 0.0001$, Kruskal Wallis test); only different treatments with the same genotype were compared (separated by grey-dashed lines). Scale bars in b to f, 5 μ m.



Extended Data Figure 5. 2x and 3xPH^{FAPP1} have longer residency time at the PM than 1xPH^{FAPP1}

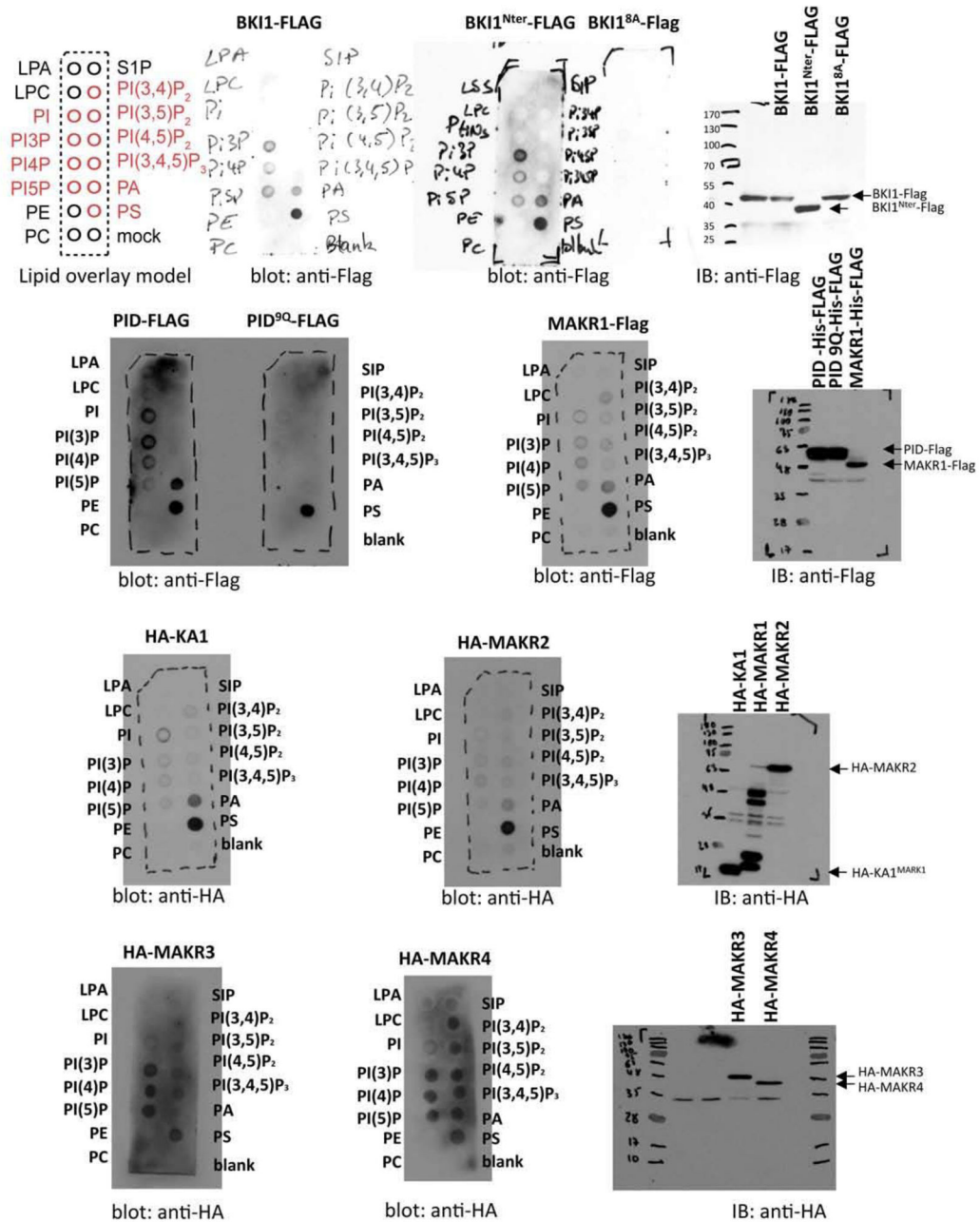
High affinity lipid binding domains (LBDs) are expected to localize more specifically to the membrane compartment that accumulates the most its cognate lipid, while lower affinity LBDs are more likely to have a broader localization domain (a–c). Low affinity sensors (here 1xPH^{FAPP1}) are less efficient in discriminating between two membranes with two different concentrations of their targeted lipid species (here PI4P) and as a result they might be targeted to both of these membranes (a). By contrast, high affinity sensors (2xPH^{FAPP1} and 3xPH^{FAPP1}) will have increased dwell time at the membrane that is the most enriched in the targeted lipid and they will accumulate preferentially in this compartment (b and c). In other words, high affinity sensors work like a “Velcro fastener”: they will grab more strongly to a surface with more spikes (in this case the spikes being PI4P). In order to confirm that our PH^{FAPP1}-based sensors behaves according to the scenario explained above, we performed a FRAP experiment (See main Fig. 3a to c). This analysis showed that the recovery was much faster in the case of 1xPH^{FAPP1} and kymographic analysis showed that the recovery of fluorescence has an oval shape, indicating recovery from both the side (i.e. the PM) and the cytosol (Fig. 3a–c of the main text). This result is compatible with the idea that 1xPH^{FAPP1} has a fast exchange rate between the PM and the cytosol. On the contrary, in the case of 2xPH^{FAPP1} and 3xPH^{FAPP1} the recovery was slower and kymographic analysis (Fig. 3b of the main text) showed that the recovery of fluorescence is centripetal (triangle shape). 1xPH^{FAPP1} localizes at the PM and in endomembranes, while 2x and 3xPH^{FAPP1} are not (or less) present in intracellular compartments. Therefore, it is conceivable that the fast recovery of the 1xPH^{FAPP1} reporter might come from fast endocytic recycling that is not happening in the case of the 2x and 3xPH^{FAPP1} proteins. To exclude this possibility, we tested whether pharmacological inhibition of protein recycling by BFA had any impact on

the recovery time of the 1xPH^{FAPP1} construct and (d–e). We found that cYFP-1xPH^{FAPP1} had similar recovery time in the presence or absence of BFA (100 μ M 60 min). These results are consistent with the notion that the 2xPH^{FAPP1} and 3xPH^{FAPP1} sensors have a longer residency time at the PM than 1xPH^{FAPP1} and repopulate the bleached area by lateral diffusion with their cognate lipids.



Extended Data Figure 6. P4M^{SidM} is specifically localized to the PM in various cell types in Arabidopsis

Confocal pictures of **a**) the root and **b**) the shoot of transgenic Arabidopsis lines stably expressing cYFP-P4M^{SidM}. Scale bars, 10 μ m.

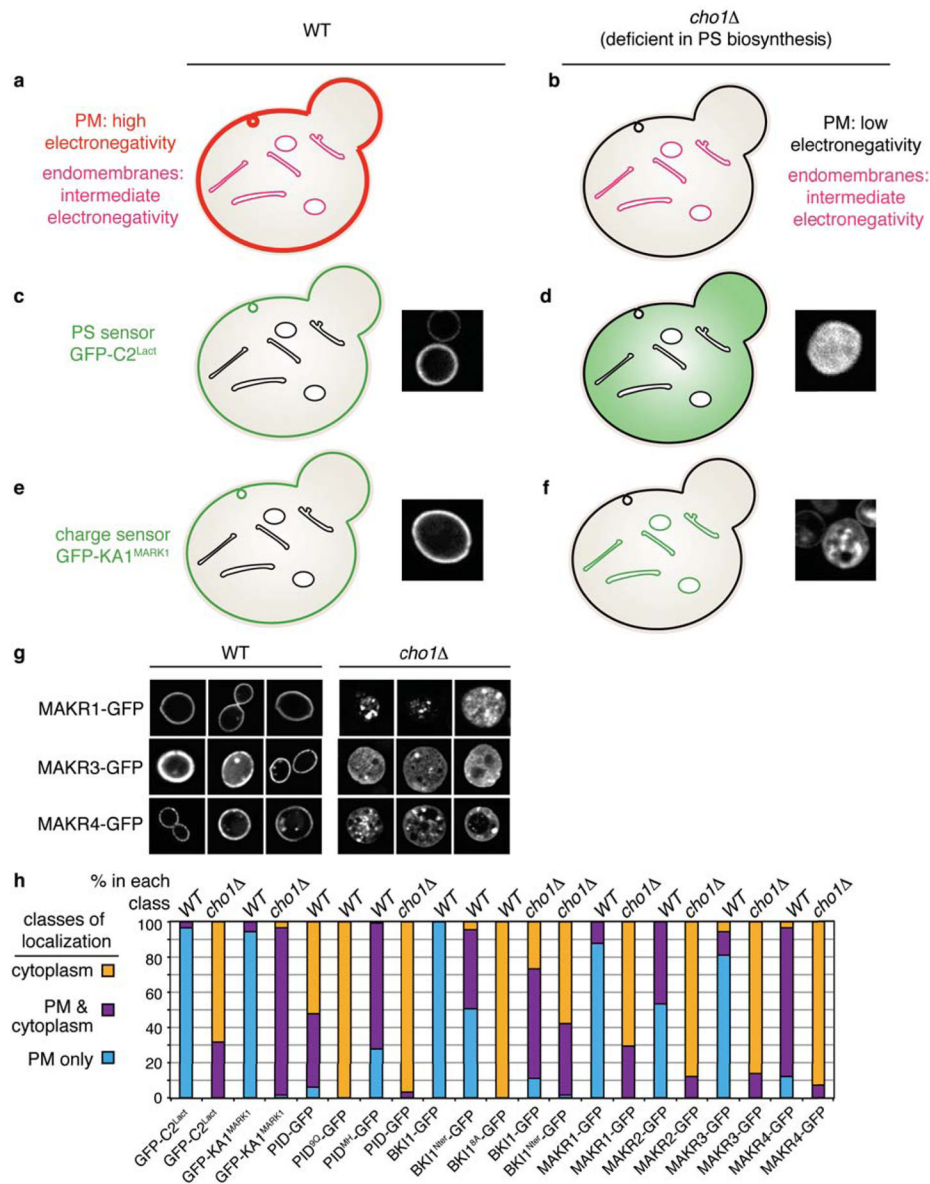


Extended Data Figure 7. Full scan of lipid-protein overlay experiments and associated western blots

Full scan of lipid overlay assays presented in the main Figure 5a, and their associated western blots. Top left is shown the position of the different lipids spotted on each membrane: Lysophosphatidic acid (LPA), Lysophosphocholine (LPC), Phosphatidylinositol (PI), Phosphatidylinositol-3-phosphate (PI3P), Phosphatidylinositol-4-phosphate (P4P), Phosphatidylinositol-5-phosphate (PI5P), Phosphatidylethanolamine (PE), Phosphatidylcholine (PC), Sphingosine 1-Phosphate (S1P), Phosphatidylinositol-3,4-bisphosphate (PI(3,4)P₂), Phosphatidylinositol-3,5-bisphosphate (PI(3,5)P₂), Phosphatidylinositol-4,5-bisphosphate (PI(4,5)P₂), Phosphatidylinositol-3,4,5-trisphosphate

(PI(3,4,5)P₃), Phosphatidic acid (PA), Phosphatidylserine (PS) and mock. Anionic phospholipids are indicated in red.

Note that with this in vitro interaction technique, we systematically found a stronger signal with PS and to a lesser extent with PA. This was also the case for HA-KA1^{MARK1} which is known to bind PS, PA and PI(4,5)P₂ with similar binding affinities in Surface Plasmon Resonance experiments². It is important to point out that these fat blots experiments are qualitative rather than quantitative. The main point of these experiments is to show that PID, BKI1 and MAKR1 to MAKR4 are indeed able to bind anionic phospholipids in vitro, and that this binding relies on their respective membrane hook (for PID and BKI1). We do not think that these experiments faithfully pin point particular lipid preferences. In fact, we expect PID, BKI1 and MAKR1 to MAKR4 to rely on membrane surface charges (non specific electrostatic interactions) in vivo and we therefore concentrated our experiments using in vivo assays (see yeast and in planta experiments).

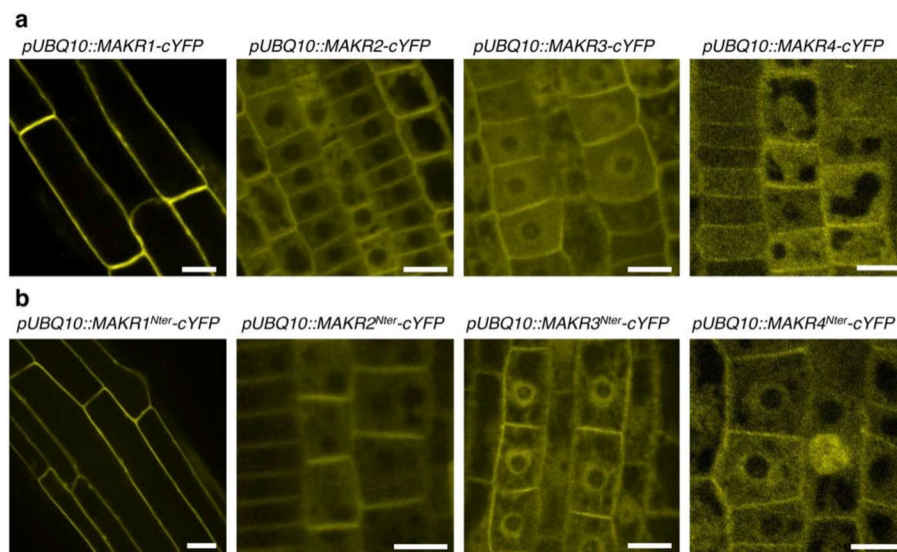


Extended Data Figure 8. Using the *cho1* yeast mutant to test the requirement of PM MSC for protein localization

a) In yeast, the PM is highly electronegative, mainly due to the presence of phosphatidylserine (PS), which massively accumulates in this membrane³. Endomembrane compartments are of intermediate electronegativity, likely because of the marginal presence anionic lipids in these compartments (e.g. PI4P in the Golgi, PI3P in endosomes). **b**) The yeast *cho1* mutant is impaired in PS biosynthesis and therefore lacks a strong PM electrostatic field^{2,3}. As a result of this loss of PM MSC, endomembranes become more electronegative than the PM in *cho1* and cationic proteins relocalize to endomembranes at the expense of the PM². This situation is exemplified by the localization of GFP-C2^{Lact} (**c** and **d**), a PS biosensor³, and GFP-KA1^{MARK1} (**e** and **f**), a MSC reporter². **c**) GFP-C2^{Lact} is specifically localized at the PM in yeast³ confirming that the main pool of this lipid is in this

membrane. **d)** On the contrary, GFP-C2^{Lact} is soluble in the *cho1*. This soluble GFP-C2^{Lact} is a localization by default in the absence of PS to target this sensor to membranes. **e)** GFP-KA1^{MARK1} is localized at the PM in yeast², confirming that the PM is highly electronegative in this system. **f)** GFP-KA1^{MARK1} is sensitive to PS depletion and relocalizes to endomembranes in the *cho1*, which become more electronegative than the PM in this mutant². Therefore, the *cho1* mutant assay allows discriminating between proteins that are targeted to the PM by specific interactions with PS (e.g. C2^{Lact}) or by reading-out the PS-dependent PM MSC (e.g. KA1^{MARK1}). Proteins that specifically interact with PS are solubilized in *cho1*, while MSC effector proteins are depleted from the PM and relocalize to endomembranes.

g) Three representative images showing the localization of the indicated constructs in WT and *cho1* yeast. **h)** Quantification of localization of the indicated construct in yeast. Cytoplasm = cytosol and/or endomembrane (n=300 cells). The localization quantification was performed using three categories according on the fluorescence expression pattern, “Plasma membrane”, “Cytoplasm” and “Plasma membrane and Cytoplasm”. Here, we took cytoplasm in a broad sense, including both soluble proteins (see for example localization of BKI1^{8A}-GFP in WT yeast or localization of the PS sensor GFP-C2^{Lact} in *cho1*) but also proteins associated with endomembranes (see for example localization of GFP-KA1^{MARK1} in *cho1*). For each GFP-tagged proteins, three independent experiments were performed and the localization was recorded in 100 yeasts in each experiment (300 cells total). Note that PID-GFP has a dual localization in yeast at the PM and in endomembrane compartments. PID^{MH}-GFP is more specifically localized at the PM than full length PID-GFP, while PID^{9Q}-GFP is localized in endomembrane compartments but not at the PM. These results suggest that in yeast PID likely has two localization sequences, one PM targeting sequence that corresponds to PID^{MH} and a second, so far unknown sequence, that targets PID to endomembranes. The situation is likely similar in planta, since PID-cYFP has a dual PM and endosomal localization, while PID^{9Q}-cYFP localizes only to endosomes but not at the PM (see Fig. 5c and 6b of the main text).



Extended Data Figure 9. Localization of MAKR1 to MAKR4 and their respective C-terminal deletion in Arabidopsis root

a) Representative images of full length MAKR1 to MAKR4 localization in roots of stably transformed transgenic Arabidopsis lines. **b)** Representative images of MAKR1 to MAKR4 N-terminus localization in root of stably transformed transgenic Arabidopsis lines. Note that, similar to BKI1, all the MAKR proteins are localized to the PM and cytoplasm. Furthermore, in some cases they are also present in the nucleus (see for example MAKR3 or MAKR4). Nuclear localization has also been reported for GFP-MAKR4 but the functional significance of this localization is currently unknown²⁴. Scale bars, 10 μ m.

Supplementary Material

Refer to Web version on PubMed Central for supplementary material.

Acknowledgments

We thank M. Dreux, O. Hamant, G. Vert, T. Vernoux, S. Mongrand, A. Martiniere-Delaunay and the SiCE group for discussions and comments, J. Chory for initial support and discussions, S. Grinstein, M. Lemmon, G. Hammond, J. Friml, J. Goedhart, B. Scheres for reagents, A. Lacroix and J. Berger for plant care and PLATIM for help with imaging. Y.J. is funded by ERC n°3363360-APPL and Marie Curie Action, n°PCIG-GA-2011-303601, under FP/2007-2013. This work was initially supported by grants from the US National Institutes of Health (GM094428) and the Howard Hughes Medical Institute to Joanne Chory and a fellowship from the H.M. Kirby foundation to Y.J. M.S is funded by a PhD fellowship from the French ministry of education. T.S is supported by ERC grant n°615739-MechanoDevo to Olivier Hamant.

References

1. Jean S, Kiger AA. Coordination between RAB GTPase and phosphoinositide regulation and functions. *Nature reviews Molecular cell biology*. 2012; 13:463–470. DOI: 10.1038/nrm3379 [PubMed: 22722608]
2. Holthuis JC, Levine TP. Lipid traffic: floppy drives and a superhighway. *Nature reviews. Molecular cell biology*. 2005; 6:209–220. DOI: 10.1038/nrm1591 [PubMed: 15738987]
3. Platre MP, Jaillais Y. Guidelines for the Use of Protein Domains in Acidic Phospholipid Imaging. *Methods Mol Biol*. 2016; 1376:175–194. DOI: 10.1007/978-1-4939-3170-5_15 [PubMed: 26552684]
4. Balla T. Phosphoinositides: tiny lipids with giant impact on cell regulation. *Physiological reviews*. 2013; 93:1019–1137. DOI: 10.1152/physrev.00028.2012 [PubMed: 23899561]
5. Kutateladze TG. Translation of the phosphoinositide code by PI effectors. *Nature chemical biology*. 2010; 6:507–513. DOI: 10.1038/nchembio.390 [PubMed: 20559318]
6. Lemmon MA. Membrane recognition by phospholipid-binding domains. *Nature reviews. Molecular cell biology*. 2008; 9:99–111. DOI: 10.1038/nrm2328 [PubMed: 18216767]
7. Bigay J, Antonny B. Curvature, lipid packing, and electrostatics of membrane organelles: defining cellular territories in determining specificity. *Developmental cell*. 2012; 23:886–895. DOI: 10.1016/j.devcel.2012.10.009 [PubMed: 23153485]
8. Cacas JL, et al. Revisiting Plant Plasma Membrane Lipids in Tobacco: A Focus on Sphingolipids. *Plant physiology*. 2016; 170:367–384. DOI: 10.1104/pp.15.00564 [PubMed: 26518342]
9. Grosjean K, Mongrand S, Beney L, Simon-Plas F, Gerbeau-Pissot P. Differential effect of plant lipids on membrane organization: specificities of phytosphingolipids and phytosterols. *The Journal of biological chemistry*. 2015; 290:5810–5825. DOI: 10.1074/jbc.M114.598805 [PubMed: 25575593]
10. Botte CY, Marechal E. Plastids with or without galactoglycerolipids. *Trends in plant science*. 2014; 19:71–78. DOI: 10.1016/j.tplants.2013.10.004 [PubMed: 24231068]

11. Boutte Y, Moreau P. Modulation of endomembranes morphodynamics in the secretory/retrograde pathways depends on lipid diversity. *Current opinion in plant biology*. 2014; 22:22–29. DOI: 10.1016/j.pbi.2014.08.004 [PubMed: 25233477]
12. Surpin M, Raikhel N. Traffic jams affect plant development and signal transduction. *Nature reviews. Molecular cell biology*. 2004; 5:100–109. DOI: 10.1038/nrm1311 [PubMed: 15040443]
13. Dettmer J, Hong-Hermesdorf A, Stierhof YD, Schumacher K. Vacuolar H⁺-ATPase activity is required for endocytic and secretory trafficking in Arabidopsis. *The Plant cell*. 2006; 18:715–730. DOI: 10.1105/tpc.105.037978 [PubMed: 16461582]
14. Grison MS, et al. Specific membrane lipid composition is important for plasmodesmata function in Arabidopsis. *The Plant cell*. 2015; 27:1228–1250. DOI: 10.1105/tpc.114.135731 [PubMed: 25818623]
15. Bayer EM, Mongrand S, Tilsner J. Specialized membrane domains of plasmodesmata, plant intercellular nanopores. *Frontiers in plant science*. 2014; 5:507. [PubMed: 25324854]
16. Yeung T, et al. Receptor activation alters inner surface potential during phagocytosis. *Science*. 2006; 313:347–351. DOI: 10.1126/science.1129551 [PubMed: 16857939]
17. Heo WD, et al. PI(3,4,5)P₃ and PI(4,5)P₂ lipids target proteins with polybasic clusters to the plasma membrane. *Science*. 2006; 314:1458–1461. DOI: 10.1126/science.1134389 [PubMed: 17095657]
18. McLaughlin S, Murray D. Plasma membrane phosphoinositide organization by protein electrostatics. *Nature*. 2005; 438:605–611. DOI: 10.1038/nature04398 [PubMed: 16319880]
19. Yeung T, et al. Membrane phosphatidylserine regulates surface charge and protein localization. *Science*. 2008; 319:210–213. DOI: 10.1126/science.1152066 [PubMed: 18187657]
20. Moravcevic K, et al. Kinase associated-1 domains drive MARK/PAR1 kinases to membrane targets by binding acidic phospholipids. *Cell*. 2010; 143:966–977. DOI: 10.1016/j.cell.2010.11.028 [PubMed: 21145462]
21. Hammond GR, et al. PI4P and PI(4,5)P₂ are essential but independent lipid determinants of membrane identity. *Science*. 2012; 337:727–730. DOI: 10.1126/science.1222483 [PubMed: 22722250]
22. Simon ML, et al. A multi-colour/multi-affinity marker set to visualize phosphoinositide dynamics in Arabidopsis. *The Plant journal: for cell and molecular biology*. 2014; 77:322–337. DOI: 10.1111/tpj.12358 [PubMed: 24147788]
23. Vermeer JE, et al. Imaging phosphatidylinositol 4-phosphate dynamics in living plant cells. *The Plant journal: for cell and molecular biology*. 2009; 57:356–372. DOI: 10.1111/j.1365-313X.2008.03679.x [PubMed: 18785997]
24. van Leeuwen W, Vermeer JE, Gadella TW Jr, Munnik T. Visualization of phosphatidylinositol 4,5-bisphosphate in the plasma membrane of suspension-cultured tobacco BY-2 cells and whole Arabidopsis seedlings. *The Plant journal: for cell and molecular biology*. 2007; 52:1014–1026. DOI: 10.1111/j.1365-313X.2007.03292.x [PubMed: 17908156]
25. Tejos R, et al. Bipolar Plasma Membrane Distribution of Phosphoinositides and Their Requirement for Auxin-Mediated Cell Polarity and Patterning in Arabidopsis. *The Plant cell*. 2014; 26:2114–2128. DOI: 10.1105/tpc.114.126185 [PubMed: 24876254]
26. Ischebeck T, et al. Phosphatidylinositol 4,5-bisphosphate influences PIN polarization by controlling clathrin-mediated membrane trafficking in Arabidopsis. *The Plant cell*. 2013; 25:4894–4911. DOI: 10.1105/tpc.113.116582 [PubMed: 24326589]
27. Caillaud MC, et al. Subcellular localization of the Hpa RxLR effector repertoire identifies a tonoplast-associated protein HaRxL17 that confers enhanced plant susceptibility. *The Plant journal: for cell and molecular biology*. 2012; 69:252–265. DOI: 10.1111/j.1365-313X.2011.04787.x [PubMed: 21914011]
28. Balla A, Tuymetova G, Tsiomenko A, Varnai P, Balla T. A plasma membrane pool of phosphatidylinositol 4-phosphate is generated by phosphatidylinositol 4-kinase type-III alpha: studies with the PH domains of the oxysterol binding protein and FAPP1. *Molecular biology of the cell*. 2005; 16:1282–1295. DOI: 10.1091/mbc.E04-07-0578 [PubMed: 15635101]
29. Delage E, Ruelland E, Guillas I, Zachowski A, Puyaubert J. Arabidopsis type-III phosphatidylinositol 4-kinases beta1 and beta2 are upstream of the phospholipase C pathway

- triggered by cold exposure. *Plant & cell physiology*. 2012; 53:565–576. DOI: 10.1093/pcp/pcs011 [PubMed: 22318862]
30. Jaillais Y, Fobis-Loisy I, Miege C, Rollin C, Gaude T. AtSNX1 defines an endosome for auxin-carrier trafficking in Arabidopsis. *Nature*. 2006; 443:106–109. DOI: 10.1038/nature05046 [PubMed: 16936718]
 31. Fujimoto M, Suda Y, Vernhettes S, Nakano A, Ueda T. Phosphatidylinositol 3-kinase and 4-kinase have distinct roles in intracellular trafficking of cellulose synthase complexes in Arabidopsis thaliana. *Plant & cell physiology*. 2015; 56:287–298. DOI: 10.1093/pcp/pcu195 [PubMed: 25516570]
 32. Thole JM, Vermeer JE, Zhang Y, Gadella TW Jr, Nielsen E. Root hair defective4 encodes a phosphatidylinositol-4-phosphate phosphatase required for proper root hair development in Arabidopsis thaliana. *The Plant cell*. 2008; 20:381–395. DOI: 10.1105/tpc.107.054304 [PubMed: 18281508]
 33. Munnik T, Nielsen E. Green light for polyphosphoinositide signals in plants. *Current opinion in plant biology*. 2011; 14:489–497. DOI: 10.1016/j.pbi.2011.06.007 [PubMed: 21775194]
 34. Hammond GR, Machner MP, Balla T. A novel probe for phosphatidylinositol 4-phosphate reveals multiple pools beyond the Golgi. *The Journal of cell biology*. 2014; 205:113–126. DOI: 10.1083/jcb.201312072 [PubMed: 24711504]
 35. He J, et al. Molecular basis of phosphatidylinositol 4-phosphate and ARF1 GTPase recognition by the FAPP1 pleckstrin homology (PH) domain. *The Journal of biological chemistry*. 2011; 286:18650–18657. DOI: 10.1074/jbc.M111.233015 [PubMed: 21454700]
 36. Xu J, Scheres B. Dissection of Arabidopsis ADP-RIBOSYLATION FACTOR 1 function in epidermal cell polarity. *The Plant cell*. 2005; 17:525–536. DOI: 10.1105/tpc.104.028449 [PubMed: 15659621]
 37. Martiniere A, et al. Cell wall constrains lateral diffusion of plant plasma-membrane proteins. *Proceedings of the National Academy of Sciences of the United States of America*. 2012; 109:12805–12810. DOI: 10.1073/pnas.1202040109 [PubMed: 22689944]
 38. Zegzouti H, et al. Structural and functional insights into the regulation of Arabidopsis AGC VIIIa kinases. *The Journal of biological chemistry*. 2006; 281:35520–35530. DOI: 10.1074/jbc.M605167200 [PubMed: 16973627]
 39. Barbosa IC, Schwechheimer C. Dynamic control of auxin transport-dependent growth by AGCVIII protein kinases. *Current opinion in plant biology*. 2014; 22:108–115. DOI: 10.1016/j.pbi.2014.09.010 [PubMed: 25305415]
 40. Jaillais Y, et al. Tyrosine phosphorylation controls brassinosteroid receptor activation by triggering membrane release of its kinase inhibitor. *Genes & development*. 2011; 25:232–237. DOI: 10.1101/gad.2001911 [PubMed: 21289069]
 41. Belkhadir Y, Jaillais Y. The molecular circuitry of brassinosteroid signaling. *The New phytologist*. 2015; 206:522–540. DOI: 10.1111/nph.13269 [PubMed: 25615890]
 42. Michniewicz M, et al. Antagonistic regulation of PIN phosphorylation by PP2A and PINOID directs auxin flux. *Cell*. 2007; 130:1044–1056. DOI: 10.1016/j.cell.2007.07.033 [PubMed: 17889649]
 43. Lee SH, Cho HT. PINOID positively regulates auxin efflux in Arabidopsis root hair cells and tobacco cells. *The Plant cell*. 2006; 18:1604–1616. DOI: 10.1105/tpc.105.035972 [PubMed: 16731587]
 44. Marques-Bueno MM, et al. A versatile Multisite Gateway-compatible promoter and transgenic line collection for cell type-specific functional genomics in Arabidopsis. *The Plant journal: for cell and molecular biology*. 2016; 85:320–333. DOI: 10.1111/tpj.13099 [PubMed: 26662936]
 45. Kang BH, Nielsen E, Preuss ML, Mastronarde D, Staehelin LA. Electron tomography of RabA4b- and PI-4Kbeta1-labeled trans Golgi network compartments in Arabidopsis. *Traffic*. 2011; 12:313–329. DOI: 10.1111/j.1600-0854.2010.01146.x [PubMed: 21134079]
 46. Preuss ML, et al. A role for the RabA4b effector protein PI-4Kbeta1 in polarized expansion of root hair cells in Arabidopsis thaliana. *The Journal of cell biology*. 2006; 172:991–998. DOI: 10.1083/jcb.200508116 [PubMed: 16567499]

47. Antignani V, et al. Recruitment of PLANT U-BOX13 and the PI4Kbeta1/beta2 phosphatidylinositol-4 kinases by the small GTPase RabA4B plays important roles during salicylic acid-mediated plant defense signaling in Arabidopsis. *The Plant cell*. 2015; 27:243–261. DOI: 10.1105/tpc.114.134262 [PubMed: 25634989]
48. Naramoto S, et al. Phosphoinositide-dependent regulation of VAN3 ARF-GAP localization and activity essential for vascular tissue continuity in plants. *Development*. 2009; 136:1529–1538. DOI: 10.1242/dev.030098 [PubMed: 19363154]
49. Heilmann M, Heilmann I. Plant phosphoinositides-complex networks controlling growth and adaptation. *Biochimica et biophysica acta*. 2015; 1851:759–769. DOI: 10.1016/j.bbali.2014.09.018 [PubMed: 25280638]
50. Potocky M, et al. Live-cell imaging of phosphatidic acid dynamics in pollen tubes visualized by Spo20p-derived biosensor. *The New phytologist*. 2014; 203:483–494. DOI: 10.1111/nph.12814 [PubMed: 24750036]
51. Cutler SR, Ehrhardt DW, Griffiths JS, Somerville, Random CR. GFP::cDNA fusions enable visualization of subcellular structures in cells of Arabidopsis at a high frequency. *Proceedings of the National Academy of Sciences of the United States of America*. 2000; 97:3718–3723. [PubMed: 10737809]

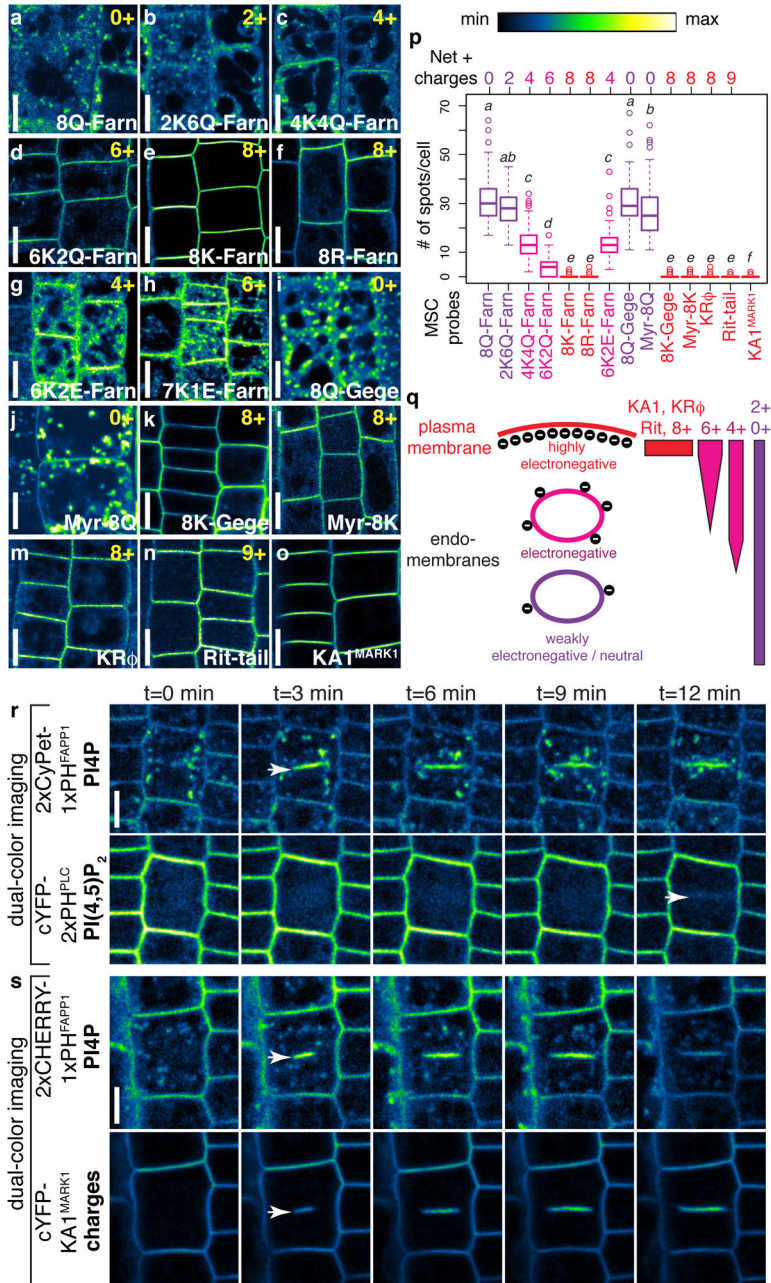


Fig. 1. The plant PM and the cell plate are highly electronegative, a property that correlates with PI4P localization

a–o) Confocal pictures of MSC probes in Arabidopsis root epidermis. Probes are indicated at the bottom and net charges at the top. **p)** Tukey boxplot showing the distribution of intracellular compartments (spots) per cell for each MSC reporter. Different italicized-letters indicate significant differences among means ($P < 0.0001$, Kruskal-Wallis test). **q)** Schematic representation of MSC organization in plants. **r–s)** Dual-color imaging during cytokinesis in Arabidopsis root epidermis. Plants co-expressing: **r)** 2xCyPet-1xPH^{FAPP1} (top) and cYFP-2xPH^{PLC} (bottom) or **s)** 2xCHERRY-1xPH^{FAPP1} (top) and cYFP-KA^{MARK1} (bottom).

Confocal images are color-coded with respect to pixel intensity based on the scale shown in the top right corner. Scale bars, 5 μm .

Author Manuscript

Author Manuscript

Author Manuscript

Author Manuscript

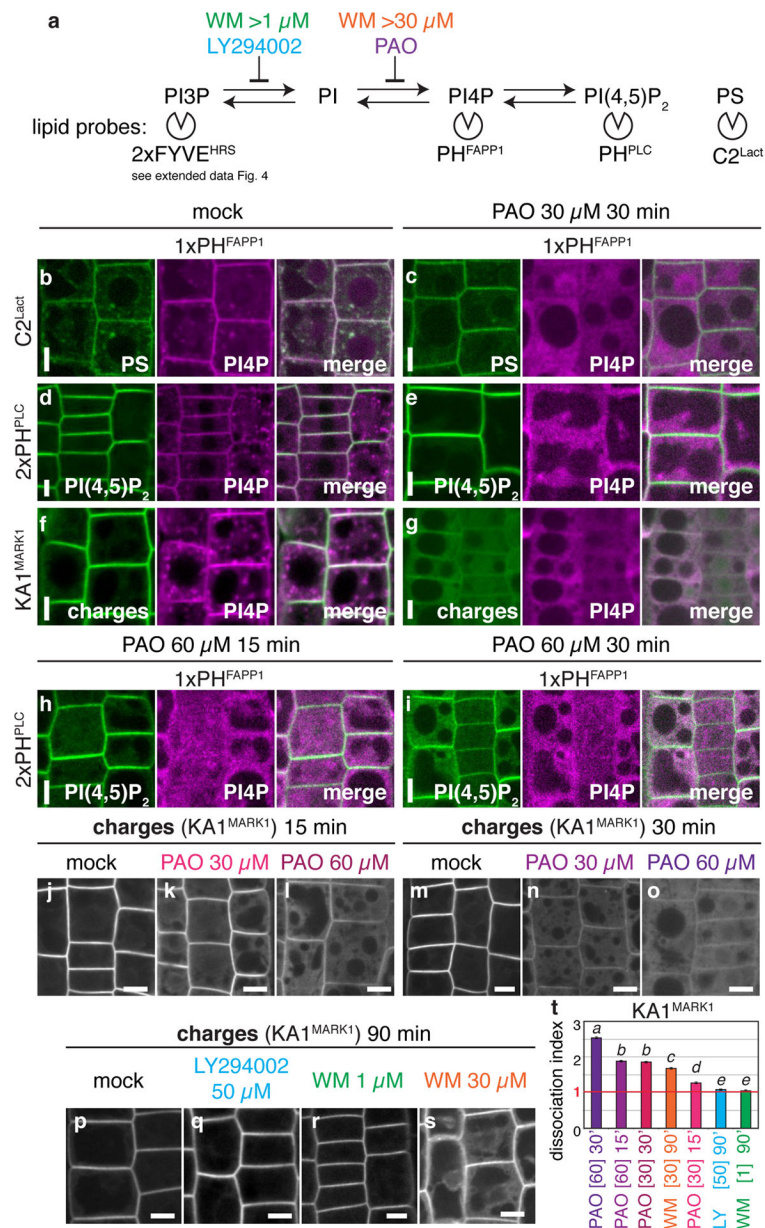


Fig. 2. PI4K activity is required to maintain the PM electrostatic signature

a) Schematic representation of the drugs used to perturb phosphoinositides production and lipid sensors used as read-out. **b–i)** Dual-color imaging of plants treated with the indicated time and drug concentration. PS, PI(4,5)P₂ and MSC reporters are pseudo-colored in green (left), 1xPH^{FAPP1} are pseudo-colored in purple (middle). Colocalizations are showed in white in the merged channel (right). **b–c)** Plants co-expressing 2xCYFP-C2^{Lact} and cYFP-1xPH^{FAPP1}. **d–e** and **h–i)** Plants co-expressing cYFP-2xPH^{PLC} and 2xCyPet-1xPH^{FAPP1}. **f–g)** Plants co-expressing cYFP-KA1^{MARK1} and 2xCYFP-1xPH^{FAPP1}. **j–s)** Confocal pictures of cYFP-KA1^{MARK1} MSC reporter treated with the indicated time and drug concentration and **t)** corresponding dissociation index

(mean \pm SEM). Different italicized-letters indicate significant differences among means ($P < 0.0001$, Kruskal-Wallis test).

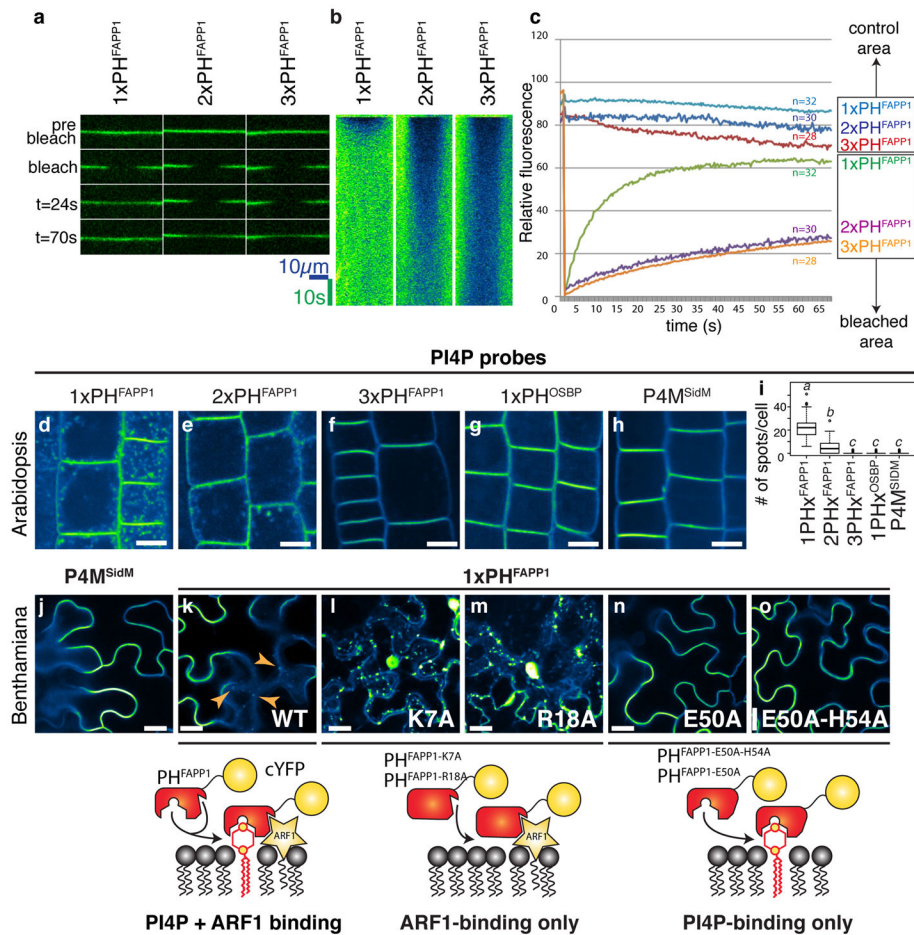


Fig. 3. PI4P is a hallmark of the plant PM

a–c) FRAP analyses of 1x, 2x and 3xPH^{FAPP1} sensors. **a)** Representative confocal pictures, **b)** kymographs of protein diffusion within the PM and **c)** trace of fluorescence intensity during FRAP analyses. **d–h)** Confocal pictures of PI4P probes in Arabidopsis root epidermis. Probes are indicated at the top. Scale bars, 5 μm. **i)** Tukey boxplot showing the distribution of intracellular compartments (spots) per cell for each PI4P reporter. Different italicized-letters indicate significant differences among means ($P < 0.0001$, Kruskal-Wallis test). **j–o)** Confocal pictures of PI4P probes in *Nicotiana benthamiana* leaf epidermis. Probes are indicated at the top and mutations in PH^{FAPP1} at the bottom. Bottom panels show schematic representations of PH^{FAPP1} membrane recruitment mechanism according to the different mutations used. Orange arrowheads indicate endosomal localization of 1xPH^{FAPP1}. Scale bars, 20 μm.

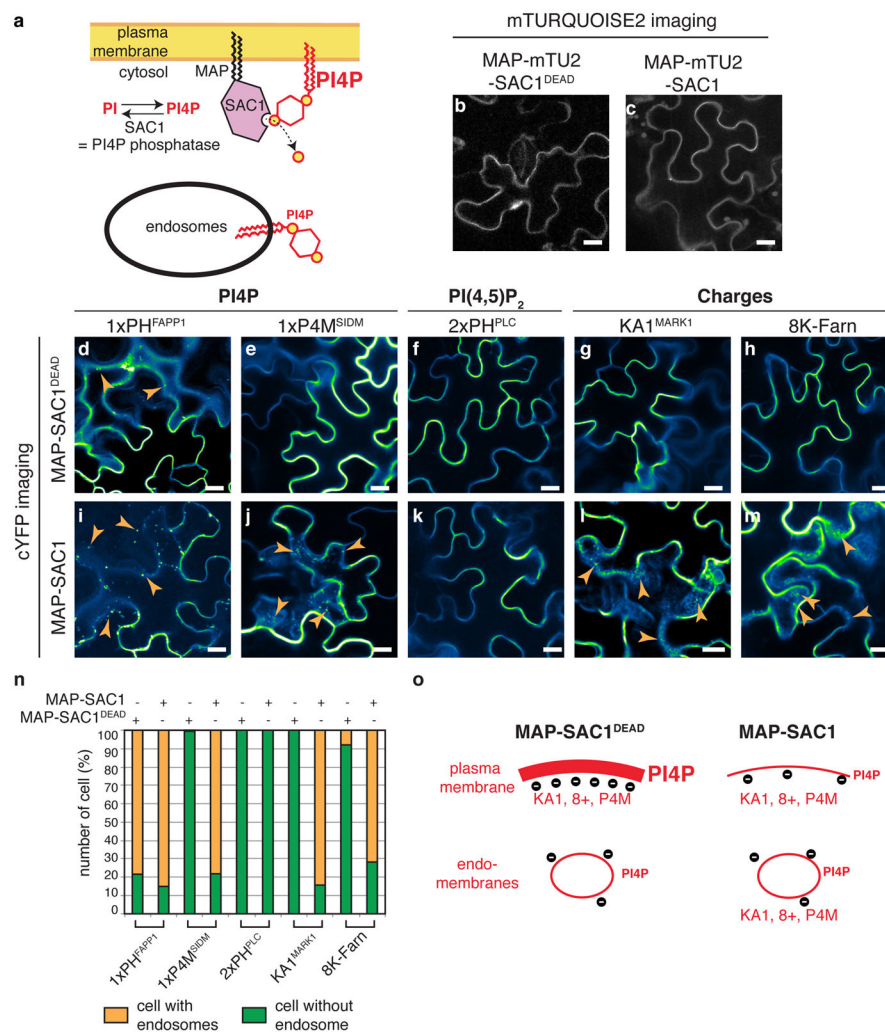


Fig. 4. PM PI4P drives the electrostatic field of the cell membrane

a) Schematic representation of the genetic system used to specifically deplete PM PI4P. **b–c)** mTURQUOISE2 imaging of MAP-mTU2-SAC1^{DEAD} (**b**) and MAP-mTU2-SAC1 (**c**) in *Nicotiana benthamiana* leaf epidermis. **d–m)** cYFP imaging of the lipid or MSC reporter indicated at the top in *Nicotiana benthamiana* leaf epidermis, co-expressed with MAP-mTU2-SAC1^{DEAD} (**d–h**) or MAP-mTU2-SAC1 (**i–m**). **n)** Quantification of localization observed in **d–m**. **o)** Schematic representation of PI4P and MSC organization in non-perturbed cells (left) or cells with reduced PM PI4P (right). Scale bars, 20 μ m.

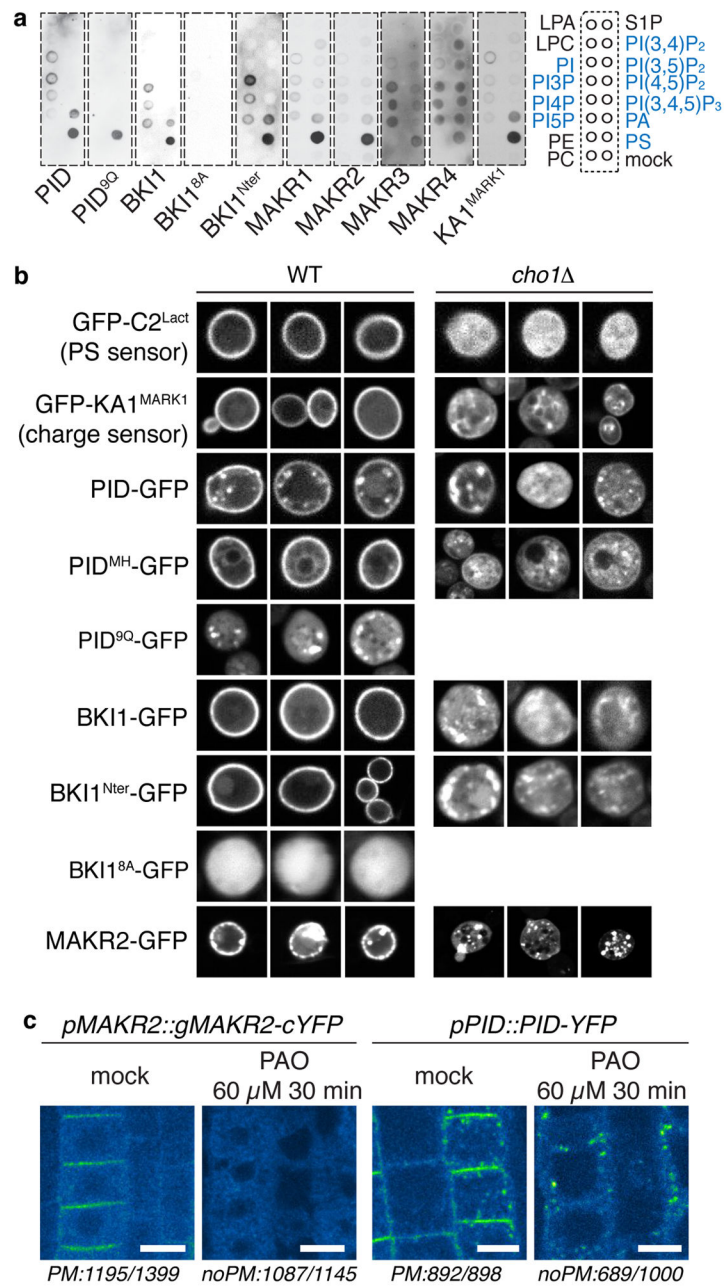


Fig. 5. PINOID and BKI1/MAKRs are effectors of the PM electrostatic field

a) Lipid overlay assays with recombinant PID-Flag, PID^{9Q}-FLAG, BKI1-Flag, BKI1^{8A}-Flag, BKI1^{Nter}-Flag, MAKR1-Flag, HA-MAKR2, HA-MAKR3, HA-MAKR4 and the HA-KA1^{MARK1} control. Anionic lipids are indicated in blue. **b)** Three representative confocal pictures showing the localization of the indicated GFP-fused protein in WT and *cho1* yeast. **c)** Representative images in mock or PAO treated plants. Numbers at the bottom indicates the proportion of cells with signal at the PM or not. Scale bars, 5 μm.

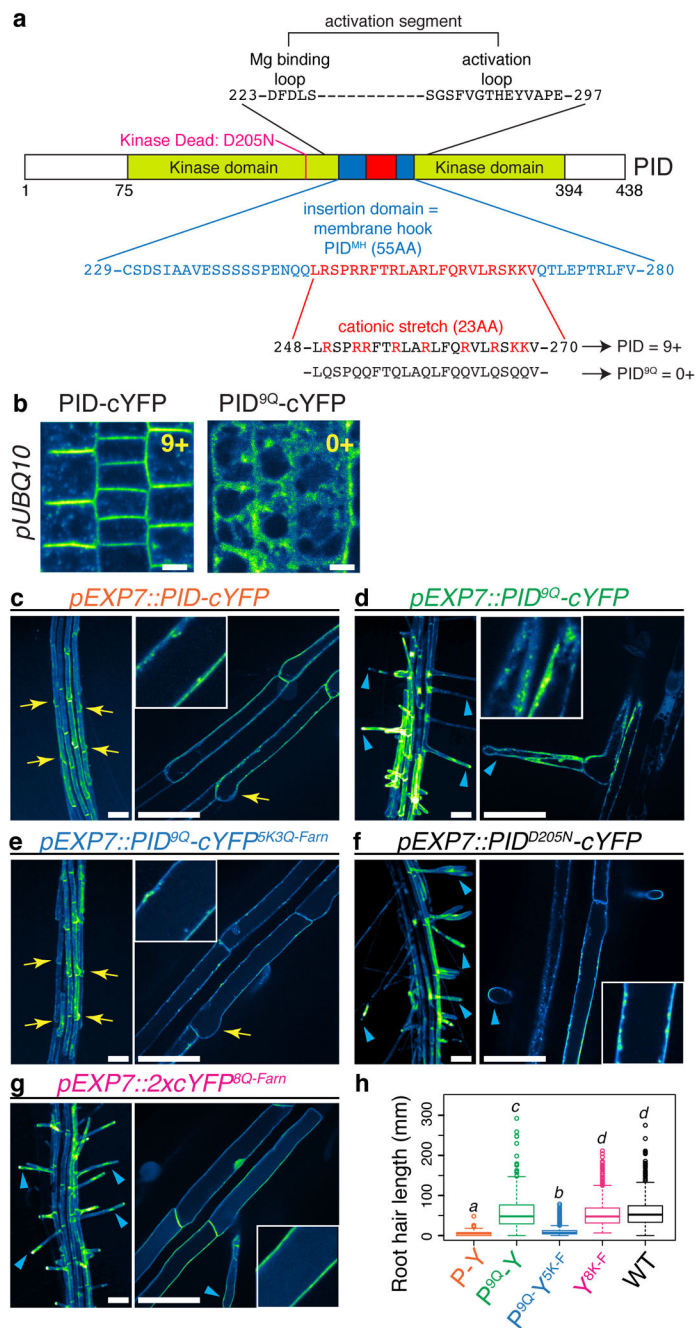


Fig. 6. PM targeting by PID cationic membrane hook is required for function

a) Schematic representation of the PID protein. **b)** Confocal picture of *pUBQ10::PID-cYFP* and *pUBQ10::PID^{9Q}-cYFP* in Arabidopsis root meristem epidermis. Scale bars, 5 μ m. **c-g)** Representative picture of root hair phenotypes (left) and localization of the indicated construct (right). Each picture was taken with identical setting indicating that each transgenic line expressed comparable level of PID protein. Blue arrowheads indicate elongated root hairs and yellow arrows indicate root hairs with inhibited growth. Scale bars, 100 μ m. **h)** Tukey boxplot showing the quantification of root hair length in the following

lines: *pEXP7::PID-cYFP* (P-Y, orange); *pEXP7::PID^{9Q}-cYFP* (P^{9Q}-Y); *pEXP7::PID^{9Q}-cYFP^{5K3Q-Farn}* (P^{9Q}-Y^{5K-F}); *pEXP7::2x-cYFP^{8K-Farn}* (Y^{8K-F}) and WT. Different italicized-letters indicate significant differences among means ($P < 0.0001$, Kruskal-Wallis test).

Author Manuscript

Author Manuscript

Author Manuscript

Author Manuscript